# Simulations of Sulfate-Nitrate-Ammonium (SNA) aerosols during the extreme haze events over Northern China in October 2014

Dan Chen[1], Zhiquan Liu[1], Jerome Fast[2], Junmei Ban[1]

[1]National Center for Atmospheric Research, Boulder, Colorado, USA

[2]Pacific Northwest National Laboratory, Richland, WA 99352

*Correspondence to:* Zhiquan Liu (liuz@ucar.edu) and Dan Chen (dchen@ucar.edu)

**Abstract:**

Extreme haze events have occurred frequently over China in recent years. Although many studies have investigated the formation mechanisms associated with $PM_{2.5}$ for heavily polluted regions in China based on observational data, adequately predicting peak $PM_{2.5}$ concentrations is still challenging for regional air quality models. In this study, we evaluate the performance of one configuration of the Weather Research and Forecasting model coupled with chemistry (WRF-Chem) and use the model to investigate the sensitivity of heterogeneous reactions on simulated peak sulfate, nitrate, and ammonium concentrations in the vicinity of Beijing during four extreme haze episodes in October 2014 over the North China Plain. The highest observed $PM_{2.5}$ concentration of 469 μg m$^{-3}$ occurred in Beijing. Comparisons with observations show that the model reproduced the temporal variability in $PM_{2.5}$ with the highest $PM_{2.5}$ values on polluted days (defined as days in which observed $PM_{2.5}$ is greater than 75 μg m$^{-3}$), but predictions of sulfate, nitrate, and ammonium were too low on days with the highest observed concentrations. Observational data indicate that the sulfur/nitric oxidation rates are strongly correlated with relative humidity during periods of peak $PM_{2.5}$; however, the model failed to reproduce the highest $PM_{2.5}$ concentrations due to missing heterogeneous/aqueous reactions. As the parameterizations of those heterogeneous reactions are not well established yet, estimates of $SO_2$-to-$H_2SO_4$ and $NO_2/NO_3$-to-$HNO_3$ reaction rates that depend on relative humidity were applied which improved the simulation of sulfate, nitrate, and ammonium enhancement on polluted days in terms of both concentrations and partitioning among those species. Sensitivity simulations showed that the extremely high heterogeneous reaction rates and also higher emission rates than those reported in the emission inventory were likely important factors contributing to those peak $PM_{2.5}$ concentrations.

## 1. Introduction

Anthropogenic $PM_{2.5}$ (fine particulate matter with aerodynamic diameters less than 2.5 μm) is known to play a significant role in atmospheric visibility, human health, and climate. Regional haze with extremely high $PM_{2.5}$ concentrations (exceeding the WHO standard tenfold) has become the primary air quality concern in China, especially over the North China Plain (NCP). Severe haze pollution episodes occur frequently over the NCP, especially in Beijing (e.g. Sun et al., 2015), during almost all seasons as described by Wen et al. (2015) for the summer of 2013, Liu et al. (2013) and Yang et al. (2015) for the autumns of 2011 and 2014, and Wang et al. (2014c) and Han et al. (2015) for the winters of 2013 and 2014. Those haze events provide an opportunity to test the current understanding of sources and the formation mechanisms of $PM_{2.5}$ over the NCP as represented in current air quality models. Most air quality modeling studies have focused on winter or summer periods (e.g. Wang et al., 2014a, 2016; Wang et al., 2014d; Chen et al., 2015; Zhang et al., 2015a, Zhang et al., 2015b; Zheng et al., 2015), because emissions resulting from heat production and adverse meteorological conditions during the winter and greater photochemical production rate during the summer play crucial roles in the formation of haze in the two seasons, respectively. Although observations (Wang et al., 2014b) suggest that the biomass burning associated with autumn harvest in the NCP could be an important source of $PM_{2.5}$, the formation mechanisms and the performance of models in autumn have not been thoroughly investigated.

Sulfate, nitrate, and ammonium (denoted as SNA) are the predominant inorganic species in $PM_{2.5}$. Observations during the winter of 2013 (e.g. Wang et al., 2014c) and autumn of 2014 (Yang et al., 2015) show that SNA increases rapidly during the highest haze episodes over the NCP and makes up approximately half of the total $PM_{2.5}$ mass. Based on the studies for the winter of 2013 and the autumn of 2014, this rapid SNA increasing is associated with relative humidity (RH). There are strong correlations between RH and sulfur/nitric oxidation ratios, thus the heterogeneous reactions of precursors (sulfur dioxide $SO_2$, nitrogen oxides $NO_x = NO+NO_2$) are key reactions that lead to the formation of sulfate and nitrate on the surface of particulates (e.g. Li and Shao, 2009, 2010; Li et al., 2011; Wang et al., 2012b; Zhao et al., 2013; Wang et al., 2014c; Yang et al., 2015). However, those reactions are not included in current chemical mechanisms (traditional gas-phase or aqueous-phase chemistry) in most air quality models. After identifying this deficiency, Wang et al. (2014d) and Zhang et al. (2015b) introduced and parameterized the heterogeneous uptake of $SO_2$ on deliquesced aerosols in the GEOS-Chem model and Zheng et al. (2015) comprehensively evaluated the effects of heterogeneous chemistry in the CMAQ model. Their simulations for the conditions during the 2013 winter showed great improvements when heterogeneous chemistry was included.

Precursor emissions are also important factors in determining SNA concentrations and composition. It is interesting to explore the response of SNA to precursor emission changes due to the uncertainties when applying the emission inventories in the model. Rapid changes related to historical and recent economic developments, or specific political decisions toward emission reductions are often not accounted for by emission inventories. This is particularly the case for the developing countries such as China (Richter et al., 2005). We use the latest emission inventory available for 2010, thus the changes of three precursor emissions

($SO_2$, $NO_x$, and $NH_3$) between 2010 and 2014 may not be reflected in our simulations. There is ample evidence to show that $SO_2$ emissions have decreased rapidly in recent years (especially after 2010-2011) from both bottom-up emission inventories (Lu et al., 2011; Xia et al., 2016) and satellite observations (Wang et al., 2015, Krotkov et al., 2016), driven by widely implementation of flue gas desulfurization in power plants. Around 30% reductions in $SO_2$ vertical column densities (VCD) were reported in Eastern China (Krotkov et al., 2016) from 2010 to 2014 and the reduction ratio reaches 50-60% from 2007-2008 to 2014. For $NO_x$ emissions that are primarily from vehicles and industries, inventory estimates based on both bottom-up and satellite remote sensing methods show increases nationwide before 2010 (Lamsal et al., 2011; Zhang et al., 2012; Shi et al., 2014; Krotkov et al., 2016; Xia et al., 2016) and also increases over western China before 2013 (Cui et al., 2016). The Chinese government set a 10% $NO_x$ emission reduction target in the 12th Five-Year Plan (2011-2015). Satellite observations show that the $NO_x$ emissions reached their peak in 2011 over Eastern China and then started to decrease during 2012. Compared to 2010, the $NO_x$ VCDs in 2014 decreased by 20% over Eastern China (Krotkov et al., 2016). Among the three precursors, $NH_3$ emissions that are dominated by agricultural sources have the largest uncertainty in terms of the total amount and also seasonal variations. Estimates of $NH_3$ emissions vary greatly among published papers (Streets et al., 2003; Kim et al., 2006; Dong et al., 2010; Zhang et al., 2010; Huang et al., 2012; Xu et al., 2015). Using the GEOS-Chem model, Wang et al. (2013) and Zhang et al. (2015b) concluded that $NH_3$ emission plays a critical role in the SNA simulations in the NCP. In addition to the uncertainties in the emission inventory, determining the dynamic variation in emissions due to unpredictable conditions (such as crop biomass burning) during the haze periods is also challenging.

In this study, we parameterized the SNA relevant heterogeneous reactions in WRF-Chem and conducted simulations in the NCP for a haze period in the autumn of 2014. To our best knowledge, this is the first study that $SO_2$-$NO_2$-$NO_3$ heterogeneous reactions were taken into account in WRF-Chem. We first evaluate the model results using available surface observations. Then, the relative importance of precursor emissions and the missing heterogeneous chemistry on the simulated results are quantified. We also conducted sensitivity simulations of heterogeneous reaction rates and precursor emissions. The model configuration, observations, and methodology of how heterogeneous reactions are treated are described in section 2. In section 3 and 4, the model evaluation and sensitivity analysis for heterogeneous reaction rates and precursor emissions are presented respectively. The concluding remarks are given in section 5.

## 2. Model description, observations, and methodology

### 2.1 WRF-Chem model

The Weather Research and Forecasting (WRF) model coupled with online chemistry (WRF-Chem) is based upon the non-hydrostatic WRF community model (http://www.wrf-model.org/index.php). Details of the WRF-Chem model are described by Grell et al. (2005) and Fast et al. (2006), and there have been many subsequent papers describing recent updates. We used version 3.6.1 in this study and a summary of physical parameterization options is shown in Table 1. The model domain with a 40-km horizontal grid spacing covers most of China and the surrounding region (left panel in Fig. 1) and our interest is the NCP (right panel in Fig. 1).

There are 57 vertical levels extending from the surface to 10 hPa. The WRF single-moment 6-class microphysics scheme (Grell and Devenyi, 2002) and the Grell-3D cumulus parameterization were used to treat clouds and precipitation. The Noah parameterization is used to represent land surface processes and the YSU parameterization is used to represent boundary layer turbulent mixing (Hong et al., 2006). Initial conditions for meteorological variables are obtained from the National Center for Environmental Prediction's (NCEP) Global Forecast System (GFS) analyses that are updated every 6 hours. The lateral boundary conditions (LBCs) for the meteorological fields are also provided by the GFS analyses. LBCs for chemistry and aerosol fields are based on prescribed idealized profiles. The simulation started on October 1, 2014 and the first three days are treated as a spin-up period and are not used in our analyses.

The Carbon-Bond Mechanism version Z (CBMZ) and Model for Simulating Aerosol Interactions and Chemistry (MOSAIC) are used as the gas-phase and aerosol chemical mechanisms, respectively, in this study. Aerosol species in MOSAIC are defined as black carbon, organic compounds, sulfate, nitrate, ammonium, sodium and chloride and other inorganic compounds. MOSAIC uses a sectional approach to represent the aerosol size distribution with 4 and 8 size bins available in the public version of the code. Research versions of MOSAIC have used up to 20 size bins in WRF-Chem (Lupascu et al., 2015). In this study, we use 4 size bins with aerosols diameters ranging from 0.039-0.1, 0.1-1, 1-2.5, and 2.5-10 μm. The Fast-J photolysis scheme is used for photolytic rate calculations. In the standard simulation with the CBMZ-MOSAIC mechanism, the SNA aerosol formation is through oxidation and neutralization/condensation of precursor gases. The sulfate formation starts from the $SO_2$ to sulfuric acid ($H_2SO_4$) oxidation, including two pathways in the model, the gas-phase oxidation of $SO_2$ by hydroxyl radicals (OH), hydrogen peroxide ($H_2O_2$) and ozone ($O_3$), and aqueous-phase oxidation of $SO_2$ by $H_2O_2$ and $O_3$ in clouds. The nitrate formation ($NO_x$ to nitric acid $HNO_3$ oxidation) also includes two pathways: the $NO_2$ oxidation by OH during the daytime and the newly added hydrolysis of dinitrogen pentoxide ($N_2O_5$) at night (Archer-Nicholls et al., 2014). $H_2SO_4$ and $HNO_3$ are neutralized/condensed mainly by/with $NH_3$ to form $(NH_4)_2SO_4$ and $NH_4NO_3$ respectively. As $H_2SO_4$ is nonvolatile, the equilibrium surface concentration is assumed to be zero in the model. $(NH_4)_2SO_4$ is the preferential species in the completion when $H_2SO_4$ and $HNO_3$ are both present and $NH_4NO_3$ is formed only if excess $NH_3$ is available beyond the sulfate requirement. Thus the amount of $NH_3$ is a key factor in determining the SNA aerosol formation in the $NH_3$-limited environment.

**Table 1.** WRF-Chem model configurations.

| | |
|---|---|
| Aerosol scheme | MOSAIC (4 bins) (Zaveri *et al.*, 2008) |
| Photolysis scheme | Fast-J (Wild *et al.*, 2000) |
| Gas phase chemistry | CBM-Z (Zavier *et al.*, 1999) |
| Cumulus parameterization | Grell 3D scheme |
| Short-wave radiation | Goddard Space Flight Center Shortwave radiation scheme (Chou and Suarez, 1994) |
| Long-wave radiation | RRTM (Mlawer *et al.*, 1997) |
| Microphysics | Single-Moment 6-class scheme (Grell and Devenyi, 2002) |
| Land-surface model | NOAH LSM (Chen and Dudhia, 2001) |

| | |
|---|---|
| Boundary layer scheme | YSU  (Hong *et al*., 2006) |
| Meteorology initial and boundary conditions | GFS analysis and forecast every 6 hour |
| Initial condition for chemical species | 3-day spin-up |
| Boundary conditions for chemical species | averages of mid-latitude aircraft profiles (McKeen *et al*., 2002) |
| Dust and sea salt Emissions | GOCART |

## 2.2 Emissions

The Multi-resolution Emission Inventory for China (MEIC) (Zhang et al., 2009; Lei et al., 2011; He 2012; Li et al., 2014) for October 2010 is used as the base emission scenario. The original grid spacing of this emission inventory is $0.25 \times 0.25$ degrees and it has been processed to match the model grid spacing (40 km). The gas precursor emissions over China for October are estimated to be 2.03 Tg for $SO_2$, 2.07 Tg for $NO_x$ ($NO_2$+NO), and 0.63 Tg for $NH_3$ in the base emission scenario and the values over the NCP are 0.60 Tg (9.32 Gmol) $SO_2$, 0.63 Tg (13.8 Gmol) $NO_x$ and 0.13 Tg (7.8 Gmol) $NH_3$ respectively. The spatial distributions of these three species are shown in Fig. 2. On the molecular basis, $NH_3$ emissions were less than the sum of $2*SO_2$ and $NO_x$ emissions indicating $NH_3$-limited conditions over the NCP.

The MEIC-2010 emission inventory has already been applied in other studies (e.g. Wang et al., 2014a, 2016; Zheng et al., 2015) for simulations over the NCP during the winter of 2013. They found that this inventory provides reasonable estimates of total emissions from cities over the NCP but is subject to uncertainties in the spatial allocations of these emissions over small spatial scales. For our simulation, uncertainties may also arise from two other aspects: the difference between the emission base year and our simulation year, and the monthly allocations (especially for $NH_3$). To address these uncertainties, sensitivity simulations are performed that alters the emission rates as described in section 2.5.

## 2.3 Observations

The meteorological data used for all the sites in the NCP are obtained from the National Climate Data Center (NCDC) integrated surface database (http://www.ncdc.noaa.gov/data-access/), shown as red circles in Fig. 1. The following parameters were evaluated: temperature and relative humidity at 2-m (T2 and RH2), wind speed and direction at 10-m (WS10 and WD10) and 24-hr accumulated precipitation.  Most of the data are of 3-hour frequency (instantaneous every 3 hours) except for precipitation. Since there is no meteorological data at sites where hourly $PM_{2.5}$ species were observed, the hourly data of T2 and RH2 from the Global Data Assimilation System (GDAS) and boundary layer height from the NOAA Air Resources Laboratory (http://www.arl.noaa.gov/index.php) at those $PM_{2.5}$ locations were used for evaluation purposes. The meteorological performance is quantified in terms of both site-by-site and also domain-wide overall statistics. The statistical measures calculated include the mean bias (MB), the root mean square error (RMSE), and the correlation (R).

The observed chemical concentrations used in the study are from three datasets: 1) the daily mean concentration of gas phase and $PM_{2.5}$ from the Air Pollution Index (API) database in 10 cities in the NCP

(shown as black dots in Fig. 1); 2) the average hourly concentrations of gas-phase pollutants and $PM_{2.5}$ at 34 monitoring sites in Beijing from the China National Environmental Monitoring Center (CNEMC); and 3) the hourly $PM_{2.5}$ measured by TEOM (tapered element oscillating microbalance, RP1405F) and 15-min species concentrations (BC, sulfate, nitrate, ammonium) in $PM_1$ measured in situ by an Aerosol Chemical Speciation Monitor (ACSM) at the Beijing Normal University (BNU, blue dot in Fig. 1) from Yang et al. (2015). Details of the BNU instruments can be found in Sun et al. (2013). As the 34 monitoring sites in Beijing fall into 8 model grids, the observations within the same grid are averaged and then the averages of the 8 grids are compared with the model predictions. There were also 5 monitoring sites in the grid cell where the BNU site is located. The average $SO_2$ and $NO_2$ among the 5 sites are also used for oxidation rates calculations.

## 2.4 Heterogeneous reactions

As discussed in section 2.1, there are several pathways for SNA formations in the standard version of WRF-Chem. Although aqueous phase processes within clouds affect sulfate, we found that the precipitation and cloud amounts in October 2014 are very low from both observation and model. Observed averaged 24-hr precipitation is less than 0.25 mm and 4 mm in Beijing and over the NCP, respectively, and the hourly cloud liquid water path is less than 10 $g/m^2$. Thus, the cloud-borne aerosols were not taken into account. For the other three oxidation pathways ($SO_2+OH \rightarrow H_2SO_4$, $NO_2+OH \rightarrow HNO_3$, $NO_2+N_2O_5 \rightarrow HNO_3$), increasing the reaction constant/rates will lead to unreasonable high values during non-haze days. Thus, the original SNA formation pathways in the model are not sufficient to explain the observed sulfate concentrations.

Following the same methodology as in Zheng et al. (2015), we added three new heterogeneous reactions into the CBMZ-MOSAIC chemical mechanism (see Table 2). These reactions are parameterized using the pseudo-first-order rate constant and is assumed to be irreversible (Zhang and Carmichael, 1999; Jacob, 2000). The rate constant k ($s^{-1}$) for the loss of gaseous pollutants is determined by (Jacob et al., 2000; Wang et al., 2012a).

$$k_i = \left(\frac{d_p}{2D_i} + \frac{4}{v_i\gamma_i}\right)^{-1} S_p, \qquad (1)$$

where the subscript $i$ represents the $i^{th}$ reactant for heterogeneous reactions, $d_p$ is the effective diameter of the particles (m), $D_i$ is the gas-phase molecular diffusion coefficient for reactant $i$ ($m^2s^{-1}$), $v_i$ is the mean molecular speed of reactant $i$ in the gas phase, $\gamma_i$ is the uptake coefficient for reactant $i$ (dimensionless) and $S_p$ is the aerosol surface area per unit volume of air ($m^2 m^{-3}$).

**Table 2.** Reactions and uptake coefficients added in this study

| Species | Reactions | Uptake coefficients (lower limit) | Uptake coefficients (upper limit) |
|---------|-----------|-----------------------------------|-----------------------------------|
| $SO_2$ | $SO_2$ (gas) + aerosol -> $SO_4^{2-}$ | $2.0 \times 10^{-5}$ | $5.0 \times 10^{-5}$ |
| $NO_2$ | $NO_2$ (gas) + aerosol -> $NO_3^-$ | $4.4 \times 10^{-5}$ | $2 \times 10^{-4}$ |

| NO$_3$ | NO$_3$ (gas) + aerosol -> NO$_3^-$ | 0.23 | 0.23 |

For the most important parameter – uptake coefficients $\gamma_i$, we used a similar method as in Wang et al. (2012a) and Zheng et al. (2015). The lower and upper limits are used to present a range of $\gamma$ values in the laboratory measurements which were applied when RH is lower than 50% and higher than 90%, respectively. The values in the 50-90% RH range are linearly interpolated based on the two limits. The lower and upper limits of NO$_2$- and NO$_3$-related reactions are based on Wang et al. (2012a) and those of SO$_2$-related reaction are based on Zheng et al. (2015)  (Table 2). We also performed sensitivity tests for those parameters as described in section 2.5.

## 2.5 Scenarios

We conducted several experiments aiming to test the model response to different heterogeneous uptake coefficients and different precursor emissions (see Table 3). The baseline emissions used in BASE and HET_BASE simulations are described in section 2.2. The heterogeneous reactions parameterization depending on RH is described in section 2.4. To determine the appropriate reaction rates, we first separated the impacts of SO$_2$ and NO$_2$-NO$_3$ relevant heterogeneous reactions on SNA simulations by turning off the NO$_2$-NO$_3$ relevant reactions in different simulations (Figure S1). We found that with only the SO$_2$ heterogeneous reactions simulated nitrate decrease due to competition of $SO_4^{2-}$ and $NO_3^-$ to form sulfate and nitrate, respectively, in NH$_3$-limited conditions. Thus, we decided to include both SO$_2$ and NO$_2$-NO$_3$ heterogeneous reactions in the simulation. We then tested several uptake coefficients as in Wang et al. (2012a). The upper and lower values used in HET_BASE are listed in Table 2. When conducting the emission sensitivity scenarios, we took into account the trends of the national emission in recent years and their uncertainties. According to the annual National Environmental Statistical Report, the total amount of SO$_2$ emissions in China reached the peak in 2006 and subsequently decreased (by ~25% from 2006 to 2014 nationally). As the MEIC-2010 emissions inventory relied on the annual statistical books in which the data is often 2-3 years older than the actual year, we assumed that the SO$_2$ emission levels in MEIC-2010 were closer to the previous 2-3 years (2007-2008). In the NCP where more strict measurements were implemented, larger-than-national-average reduction ratios were expected. For the above reasons, we applied 25% reduction of SO$_2$ in the HET_EMIS scenario. Since the NCP is in NH$_3$-limited conditions, we increased the NH$_3$ emission by 30% to test the sensitivity in HET_EMIS. The emission changes were applied to the whole modeling domain. It should be noted that the NCP is still under NH$_3$-sensitive condition after applying the SO$_2$ and NH$_3$ emission changes (please refer to the NCP emission totals in section 2.2)

**Table 3.** Simulation descriptions

| Simulation name | Emission | Heterogeneous reactions uptake coefficients | | |
| --- | --- | --- | --- | --- |
| | | SO$_2$ | NO$_2$ | NO$_3$ |
| **For the whole month of Oct.** | | | | |
| **BASE** | BASE | Heterogeneous reactions not applied | | |
| **HET_BASE** | BASE | $2.0 \times 10^{-5}$ | $4.4 \times 10^{-5}$ | 0.23 |

| HET_EMIS | SO$_2$ decrease by 25% NH$_3$ increase by 30% | (lower) $5.0 \times 10^{-5}$ (upper) | (lower) $2 \times 10^{-4}$ (upper) | |
|---|---|---|---|---|
| **For Oct. 24-25** | | | | |
| **HET_MAX1** | BASE | $1.5 \times 10^{-4}$ | $6 \times 10^{-4}$ | 0.69 |
| **HET_MAX1_EMIS1** | SO$_2$ decrease by 25%; NH$_3$ increase by 50%; NO increase by 50% | $1.5 \times 10^{-4}$ | $6 \times 10^{-4}$ | 0.69 |
| **For Oct. 25** | | | | |
| **HET_MAX2_EMIS2** | SO$_2$ decrease by 25%; NH$_3$ increase by 100%; NO increase by 100% | $3.5 \times 10^{-4}$ | $6 \times 10^{-4}$ | 0.69 |

We also tested three additional scenarios for the October 24-25 period, aiming to improve the simulated peak values of observed SNA aerosols during the highest polluted event. Although the emission changes in HET_EMIS may reflect some emission trends in recent years and also the uncertainty of the emission inventory, it does not account for dramatic emission increases that are possible during actual polluted events. In addition, the dependent reaction rates will be too low when the simulated RH is also too low. For these two reasons, we increased the emissions and adjusted those uptake coefficients as fixed values in HET_MAX1, HET_MAX1_EMIS1 and HET_MAX2_EMIS2. It should be noted that we did not have any evidence to determine the SO$_2$ uptake coefficient in those sensitivity simulations due to the limited observations (only one site for a few days). The values here are chosen to best match the observations. More rigorous optimization tests should be conducted in future studies.

## 3. Model evaluation

### 3.1 Meteorology

Table 4 quantifies the performance of the meteorological predictions based on the comparisons with the NCDC dataset. In addition to the averaged statistics in two regions (NCP and the whole study domain), statistics for the three sites PEK, Baoding and Shijiazhuang are also listed. PEK is the only NCDC observational site in Beijing and in our simulation it is one grid cell north of the BNU site where PM$_{2.5}$ species were observed. Baoding and Shijiazhuang are two sites generally upwind of Beijing and considered as the major PM$_{2.5}$ sources in the region. The temperature and relative humidity at 2-m are overall underestimated in both the NCP (with biases of -0.09 degree for T2 and -7.09% for RH2) and the whole domain (-0.78 degree and -1.91% respectively), while wind speed at 10-meter is overestimated with biases of 0.99 m s$^{-1}$ (27.4%) over the NCP and 0.78 m s$^{-1}$ (22.6%) over China. It should be noted that the intervals of WS10 in NCDC observations are 1 m s$^{-1}$ and the minimum valid value is 1 m s$^{-1}$ that no data is provided when wind speed is less than 1 m s$^{-1}$. This may cause some biases in the comparison especially when the simulated wind speeds are smaller than 1 m s$^{-1}$. The averaged correlations in the two regions ranged from 0.91-0.93 for the 2-m temperature (T2), 0.73-0.79 for the 2-m relative humidity (RH2), and 0.52-0.53 for the 10-m wind speed (WS10). Compared with another study focusing on the China-NCP that used nested-domains in WRF-Chem (Wang et al., 2016), the performance of meteorological simulation in both China and NCP regions are comparable in terms of similar

8

ranges of bias and RMSE, except for the simulated water vapor/RH and wind speed over the NCP. In Wang et al. (2016), the simulated wind speeds in the outer domain (36 km over China) during January 2013 were overestimated by more than 30% but the overestimation was reduced to less than 10% within the inner domain (12 km over the NCP). This suggests that nested domains may help reduce the overprediction in wind speeds. In Wang et al. (2016), water vapor was usually overestimated by 8-14% during January 2013, while the RH is underestimated by 2-7% during October 2014 in our study. Overall the statistics suggest that the meteorological performance of the model is reasonable for the NCP and the whole domain, while the overestimated wind speed may lead to some negative biases of the chemical species and the underestimated RH may also cause negative biases of RH-dependent reaction coefficients in the simulations.

For site-by-site comparisons, the monthly-mean 2-m relative humidity biases at PEK, Baoding and Shijiazhuang are -11.80, -20.29 and -16.10% respectively, which are larger than the NCP average. The biases in the 2-m temperature are also larger at the three sites (from -0.24 to 1.10 degrees). The 10-m wind speed biases are relatively lower at PEK (0.36 m s$^{-1}$) and Baoding (0.37 m s$^{-1}$) than the NCP average, but higher than the average at Shijiazhuang (1.50 m s$^{-1}$).

To clearly show the fluctuations of these meteorological parameters, the time series (in local time) of T2, RH2, WS10 and WD10 at the PEK site are shown in the left panels of Fig. 3. To illustrate the relationship of meteorology and PM$_{2.5}$, the time series of T2, RH2, PBLH and PM$_{2.5}$ at the BNU site are also shown in Figure 3 (right panels). From the comparisons at both sites, we can see that the T2, WS10 and WD10 simulations in Beijing are reasonable, but model failed to reproduce high RH on some days. Large low biases of 20-30% were produced for October 13-20, 25, and 29-31. The lowest bias occurred on October 25 when the observed RH was between 70 and 100% and the simulated values were around 50 to 70%. The model successfully captured the observed temporal variations of the boundary layer height, including the relatively low boundary layer height during most of the days and also the rapid increases (along with strong winds) on October 5, 12, 15 and 26. The time series of both the observations and simulations show strong anti-correlations for boundary layer height and PM$_{2.5}$, but positive correlations for boundary layer height and 10-m wind speed, which indicates that boundary layer height and wind patterns are the important meteorological factors that contributed to PM$_{2.5}$ accumulation in Beijing.

**Table 4.** Statistics of meteorological simulations

|  | N pairs of data | Mod. | Obs. | BIAS(Mod.-Obs.) | RMSE | R |
|---|---|---|---|---|---|---|
| **T2 (K)** | | | | | | |
| PEK | 670 | 286.26 | 286.50 | -0.24 | 1.90 | 0.90 |
| Baoding | 196 | 288.57 | 287.46 | 1.10 | 2.43 | 0.88 |
| Shijiazhuang | 196 | 288.41 | 288.79 | -0.37 | 2.80 | 0.80 |
| NCP average | 16173 | 285.28 | 285.38 | -0.09 | 2.57 | 0.91 |
| China average | 98984 | 287.03 | 287.82 | -0.78 | 3.25 | 0.93 |
| **RH2 (%)** | | | | | | |
| PEK | 670 | 54.87 | 66.67 | -11.80 | 18.48 | 0.83 |
| Baoding | 196 | 50.20 | 70.49 | -20.29 | 26.15 | 0.69 |

| | | | | | | |
|---|---|---|---|---|---|---|
| Shijiazhuang | 196 | 49.72 | 65.82 | -16.10 | 23.71 | 0.64 |
| NCP average | 16170 | 54.26 | 61.35 | -7.09 | 16.44 | 0.79 |
| China average | 98968 | 62.28 | 64.18 | -1.91 | 16.21 | 0.73 |
| **WS10 (m/s)** | | | | | | |
| PEK | 638 | 2.53 | 2.17 | 0.36 | 1.39 | 0.53 |
| Baoding | 147 | 2.38 | 2.01 | 0.37 | 1.20 | 0.56 |
| Shijiazhuang | 150 | 2.74 | 1.24 | 1.50 | 2.00 | 0.49 |
| NCP average | 14781 | 3.61 | 2.62 | 0.99 | 2.10 | 0.53 |
| China average | 91243 | 3.45 | 2.67 | 0.78 | 2.09 | 0.52 |
| **WD10 (degree)** | | | | | | |
| PEK | 480 | 168.51 | 157.75 | 10.76 | 144.97 | 0.17 |
| Baoding | 147 | 162.14 | 158.16 | 3.98 | 117.40 | 0.34 |
| Shijiazhuang | 150 | 181.38 | 199.87 | -18.48 | 120.55 | 0.30 |
| NCP average | 14552 | 188.37 | 188.09 | 0.29 | 112.66 | 0.40 |
| China average | 88387 | 165.19 | 182.36 | -17.17 | 125.28 | 0.34 |
| **24-hr Precipitation (mm)** | | | | | | |
| NCP average | 71 | 2.29 | 3.52 | -1.23 | 7.35 | 0.35 |
| China average | 603 | 3.98 | 4.17 | -0.19 | 11.14 | 0.28 |

## 3.2 PM$_{2.5}$ and gas-phase pollutants

   To evaluate the performance of the transport and chemistry in the original model configuration, the observed 24-hour averaged PM$_{2.5}$ concentrations at 10 national monitoring sites in the NCP are compared with the BASE simulation in Fig. 4. While Fig. 1 shows that PM$_{2.5}$ pollution has regional variations over the NCP, Fig. 4 illustrates four pollutant events with peak values on October 9, 19, 24, and 31 that occurred on almost the same days at those 10 cities. The correlations are most obvious for Beijing, Baoding, and Shijiazhuang. The BASE simulation reproduced the overall PM$_{2.5}$ levels and also the four peak events at these sites, but the peak values were too low. The daily mean PM$_{2.5}$ values at the three aforementioned cities are highest among the 10 cities and bias in the model is also the largest.

   Figure 5 shows the time series of observed and simulated hourly PM$_{2.5}$, PM$_{10}$, and four trace gases in the vicinity of Beijing. The observational data are averages among 34 sites. Observed NO$_2$ and carbon monoxide (CO) show four pollution events that are consistent with the high PM$_{2.5}$ events. CO is an important tracer since the local ambient concentrations depend mostly on emission rates, transport, and turbulent mixing. Simulated CO level is reasonable for relatively clean days when observed CO is less than 0.7 mg m$^{-3}$, but significantly underestimates peak values by 50-70% for the four polluted events. Since the boundary layer heights and winds are reasonably simulated (Fig. 3), it is possible that the CO emission rates were higher during these events which were not reflected in the baseline emission scenario. If we assume that CO emissions are underestimated in the baseline emission scenario for the peak days, we should also expect NO$_x$ emissions to be underestimated for these days since they both are emitted primarily from vehicles. However, the simulated NO$_2$ is reasonable, except that it is too low only on October 17-18. Simulated O$_3$ is too low during the four peak events based on

10

the averages of the 34 sites (in urban/suburban regions). $O_3$ formation is more complex as the dependence of $O_3$ production on $NO_x$ and VOCs is significantly different between the so-called $NO_x$-limited regime (in Beijing urban region) and the VOC-limited regimes (in the suburban region). For $SO_2$, the major sources are from combustion (during the heating season) and industry. Severe overestimation (around 3 times) of $SO_2$ concentrations and underestimation of other pollutants may indicate that the $SO_2$ emissions from industry are overestimated for the October simulation in Beijing, consistent with new regulations applied in recent years. As shown in Krotkov et al. (2016), 30% reductions in $SO_2$ vertical column densities were observed from OMI over Eastern China from 2010 to 2014, and the reduction ratio reaches 50-60% for the period from 2008 to 2014. The reductions in Beijing are likely larger than the Eastern China average since more strict pollution control policy was implemented. Besides, the overestimation may also indicate that the $SO_2$ oxidation is too weak/slow in the model. These comparisons not only serve as an evaluation of the simulated chemistry, but also provide some insights on how uncertainties in the emissions estimates affect the simulated values.

## 4. SNA response to heterogeneous reaction rates and precursor emissions

The observations at the BNU site provided not only hourly $PM_{2.5}$ concentrations, but also concentrations of black carbon, ammonium, nitrate, and sulfate. The latter three are valuable to investigate 1) the impacts of newly added heterogeneous reactions to SNA and $PM_{2.5}$ simulation in the model and 2) the relative role of heterogeneous reactions and precursor emissions.

Figure 6 shows the hourly $PM_{2.5}$ concentrations as well as the $PM_1$ BC, sulfate, nitrate, and ammonium concentrations between October 15-31 at the BNU site. This period covers three of the highest polluted events when $PM_{2.5}$ concentrations started to increase from very clean conditions to larger than 200-400 μg m$^{-3}$. The BASE simulation reproduced the October 27-31 event in terms of $PM_{2.5}$ and the four species, but it failed to reproduce the October 16-21 and October 21-25 events. The observed BC in $PM_1$ clearly shows the increase of primary BC emissions during the two events that the model failed to reproduce, indicating a likely underestimation of the primary $PM_{2.5}$ emission during the two events. Comparisons of SNA aerosols for the October 16-21 event show that the BASE simulation captured the SNA aerosol species with small low biases on October 20. During this event, the underestimation of $PM_{2.5}$ might be due to organic compounds and other inorganic species. While observed SNA aerosols increased dramatically starting on October 24 and almost doubled (nitrate and ammonium) or tripled (sulfate) within 48 hours during the October 21-25 event, the BASE simulations severely underestimated the SNA aerosols, especially for sulfate.

Compared with the BASE simulation, the newly added $SO_2$ heterogeneous reactions in HET_BASE simulation did increase the $PM_1$ sulfate concentrations with the largest increase occurring on October 23 when sulfate almost doubled from the BASE to HET_BASE simulations. Since the reaction rates are RH dependent, simulated sulfate was overestimated when the RH is too high on October 23. While the simulated RH is too low (Fig. 3) for the observed peak SNA event on October 24-25, the sulfate in HET_BASE did not improve too much. The sensitivity simulation results for this two-day period will be discussed later. As the competition of

11

$SO_4^{2-}$ and $NO_3^-$ to form sulfate and nitrate respectively in $NH_3$-limited conditions, new $NO_2$-$NO_3$ heterogeneous reactions should also be added in the model along with the $SO_2$ heterogeneous reactions to avoid the nitrate decrease. Compared with the BASE simulation, nitrate in HET_BASE remained nearly the same and ammonium increased slightly. Although HET_BASE changed the SNA ratios, especially the sulfate to nitrate ratio, the total $PM_{2.5}$ mass did not increase significantly. This is because Beijing is in $NH_3$-limited condition and the SNA mass is highly dependent on the $NH_3$ emissions. In HET_EMIS, the 30% $NH_3$ emission increase leads to noticeable nitrate and ammonium increases when compared to HET_BASE. Moreover, the 25% $SO_2$ emission decrease in HET_EMIS leads to slight sulfate decrease. The total $PM_{2.5}$ mass increases in HET_EMIS when compared with BASE and HET_BASE, but HET_EMIS still has a large low bias between October 24-25. The mass fraction, depicted as a pie chart in Fig. 7, more clearly illustrates the differences in the SNA ratio changes among the simulations. In this figure, composition concentrations on polluted days (when observed $PM_{2.5}$ is larger than 75 μg m$^{-3}$) are averaged between October 15-31. In the BASE simulation, the sulfate and nitrate fractions are significantly lower on polluted days. With the newly added heterogeneous reactions, the SNA fractions from HET_BASE are very close to observations.

The sulfur oxidation ratio (SOR= $nSO_4^{2-}/(nSO_4^{2-}+nSO_2)$) ($n$ refers to the molar concentration) and the nitric oxidation ratio (NOR= $nNO_3^-/(nNO_3^-+nNO_2)$) are important factors showing the gaseous species oxidation rates and the secondary transformation (Sun et al., 2006, 2013). The high fractions of sulfate and nitrate in heavily polluted episodes could be related to the high oxidation rates of SOR and NOR. Figure 8 shows the observed and simulated SOR and NOR for October 15-31 at the BNU site. The colors of those scatter points are associated with $PM_{2.5}$ concentrations. As simulated $SO_2$ were 3 times higher in Beijing compared with observations from the 34 local sites (Fig. 3) possibly due to an overestimates in the $SO_2$ emissions, the calculated SOR by the simulations would be artificially low due to the $SO_2$ overestimation. To correct this problem and to check the SOR differences among different simulations, we used the observed $SO_2$ when calculating the SOR for the BASE, HET_BASE and HET_EMIS simulations. The hypothesis is that the environment in Beijing is sulfur-rich and the $SO_2$ overestimation would be corrected by reducing the $SO_2$ emissions in the model. It should be noted that reducing $SO_2$ emissions in the model not only reduces $SO_2$ concentrations, but also aerosol sulfate concentrations which may lead to SOR decrease in the three simulations. This uncertainty should be considered when conducting the heterogeneous reaction coefficients tests in the future. From the observations we can see that SOR and NOR have a drastic increase in the 80-100% RH range and are strongly correlated with high $PM_{2.5}$ concentrations. In the BASE simulation without the heterogeneous reactions, the corrected SOR and NOR are within a reasonable range when RH is below 60%, but the corrected SOR and NOR are too low when RH is between 80-100% and 90-100%, respectively. SOR and NOR are improved in HET_BASE simulation. In HET_EMIS simulation, the increase of $NH_3$ emissions and decrease of $SO_2$ emissions lead to increased NOR and $PM_{2.5}$ total mass.

From the October 15-31 period (Fig. 6-7), we can see that the BASE simulation generally reproduced the $PM_{2.5}$ mass and also SNA species in relatively clean days, and the added heterogeneous reactions in HET_BASE helps to improve the SNA simulations (especially for sulfate) during the polluted events.

Nevertheless, there are still large biases between October 24 and 25. Given that the simulation meteorology is reasonable for these two days (Fig. 3), we assume that there might be two possible reasons for the biases: 1) the reaction rates are still too low due to the settings in the upper limit of $SO_2$ uptake coefficients and also the simulated RH, 2) the increase of precursor emissions in the upwind areas (southwestern of Beijing) are not reflected in the model as small fires from autumn biomass burning are not updated in the emission inventory. Fire count from http://rapidfire.sci.gsfc.nasa.gov/cgi-bin/imagery/firemaps.cgi, however, did show intensive fire locations in southern Hebei, which is upwind of Beijing. Another factor is that the underestimations of $PM_{2.5}$ in Shijiazhuang and Baoding on October 24-25 are even larger. To examine our assumptions, several different scenarios are (details in section 2.5) simulated for these two days and the results are shown in Fig. 9. In HET_MAX1 simulation, the reaction rates for the $SO_2$-$NO_2$-$NO_3$ heterogeneous reactions are fixed and tripled of the upper limits in HET_BASE. Without any emission increase, simulated sulfate almost reached the peak values on October 24 but were still underestimated on October 25. A higher $SO_2$ heterogeneous reaction rate (7 times of the upper limit in HET_BASE) and also doubled $NH_3$ emissions in HET_MAX2_EMIS2 enable the model to reach the sulfate peak on October 25. For nitrate, the increase of $SO_2$ heterogeneous reaction rates in HET_MAX1 lead to lower nitrate concentrations even though the $NO_2$-$NO_3$ heterogeneous reaction rates were also tripled. Only when $NO_x$ and $NH_3$ emissions in HET_MAX1_EMIS1 are increased by 50% do simulated peak nitrate concentrations become comparable with observations on October 24 and 25. Therefore, to reach the peak values of SNA aerosols on these two days, the sensitivity simulations suggest an increase of $SO_2$ heterogeneous reaction rates and $NO_x$ and $NH_3$ emissions are essential. For the best simulations (HET_MAX1_EMIS1 on October 24 and HET_MAX2_EMIS2 on October 25), total $PM_{2.5}$ mass was improved by ~100 μg m$^{-3}$ compared to the BASE simulation.

In the three scenarios for October 24-25, the $SO_2$ uptake coefficients were 3 and 7 times of the values in HET-BASE. It is hard to justify whether those values are realistic. More rigorous tests should be conducted when additional observations become available. It is also difficult to determine whether the sulfate underestimation is only due to the missing of heterogeneous reactions. Zhang et al. (2015b) also emphasized that aqueous reactions of $SO_2$ by $H_2O_2$, $O_3$ and $NO_2$ in cloud and on deliquescent aerosols would also help to improve the sulfate simulations significantly in GEOS-Chem. Following the study of Zhang et al. (2015b), we added the relevant aqueous reactions in WRF-Chem model. As there is not much precipitation and clouds during our simulation period, only the reactions ($H_2O_2$, $O_3$ and $NO_2$) on deliquescent aerosols are added. Based on a two-week simulation period (October 15-31, 2014), those aqueous reactions do increase the sulfate concentrations by 15% and 14% over the NCP and domain-wide, respectively (Fig. 10). The increase also reaches 13% in high sulfate region (central China and Sichuan). For Beijing, the newly added aqueous reactions improve the sulfate concentrations by 4.9% during clean days and 9.9% during heavy polluted days at the BNU site. It indicates that other missing reactions, in addition to the heterogeneous reactions, may also play important role in the sulfate underestimation in the model. As indicated in Zhang et al. (2015b), the transport of SNA aerosols from upwind areas is another important contributor in addition to precursor emission rates.

## 5. Conclusions

Accurately predicting the concentration and composition of particulate matter is still very challenging for climate and air quality models. In this study, the WRF-Chem model was used to simulate the high $PM_{2.5}$ events in the North China Plain (NCP) surrounding Beijing for an autumn period (October 1-31, 2014). Our objective is to evaluate the capability of one such model, better understand the mechanisms that form sulfate, investigate the uncertainties associated with a set of heterogeneous chemical reactions, and improve the simulations of very high $PM_{2.5}$ concentrations during pollution episodes. The evaluations of meteorological parameters in the NCP show that model is capable to capture the temporal variations of boundary layer height as well as the low boundary layer heights during four pollution events. The deficiencies in meteorological forecasts were underestimates in relative humidity, especially during the most polluted days, and the overestimates in wind speed. While the default version of the CBMZ-MOSAIC mechanism available in the public version of WRF-Chem was able to simulate the high $PM_{2.5}$ concentrations (daily mean up to 200 $\mu g\ m^{-3}$) for most of the cities in the NCP, the model severely underestimated the peak values (hourly mean greater than 400 $\mu g\ m^{-3}$) in Beijing and at upwind sites (Baoding and Shijiazhuang). PM species observations at BNU site in Beijing show that the sulfate-nitrate-ammonium aerosols (SNA) increases dramatically during these peak events and the increased sulfur-oxidation rates and nitric-oxidation rates are strongly correlated with the high relative humidity (60-90%) on those days.

The failure of the model to simulate the peak $PM_{2.5}$ concentrations is mainly due to the underestimation of SNA and secondary organic compounds. Analyses of the SNA underestimation revealed that missing $SO_2$-$NO_2$-$NO_3$ relevant heterogeneous reactions in the current aerosol scheme are likely important in China. Following the methodology in Zheng et al. (2014), the RH-dependent $SO_2$, $NO_2$ and $NO_3$ uptake heterogeneous reactions were added to the CBMZ-MOSAIC chemistry scheme. With the newly added reactions, the SNA simulations of the ratios of SNA in PM and the partitioning of sulfate and nitrate aerosols were improved on polluted days. However, there was still a 100 $\mu g\ m^{-3}$ underestimation of SNA aerosols for the October 24-25 period when $PM_{2.5}$ concentrations were as high as 400-500 $\mu g\ m^{-3}$. Two possible explanations are proposed: 1) The RH-dependent reaction rates of those heterogeneous reactions especially the $SO_2$ uptake reactions on those peak days were not high enough either due to the underprediction in RH or the setting of the upper limits of uptake coefficients; 2) Comparisons of modeled gas-phase precursors showed the possibility of precursor underestimation (especially $NO_x$) in the model. Although the two explanations cannot be proved definitively without additional observational evidence, sensitive simulations with increased heterogeneous reaction rates and increased $NO_x$ and $NH_3$ emissions show great improvement of SNA simulations in the model for the October 24-25 peak pollution events. In addition to the heterogeneous reactions, missing aqueous reactions may also play important role in the sulfate underestimation in the model.

We conclude that RH in the 60-100% range is a significant factor contributing to peak $PM_{2.5}$ values, especially during the heavily polluted days when sulfur and nitric oxidation rates almost doubled or tripled indicating the rapid heterogeneous reactions. With the underprediction in RH in this range and the corresponding low reaction rates, it is difficult for the model to reproduce the high concentrations of SNA. Data

assimilation of meteorological variables, particularly humidity, might be useful from this point of view. Two other concerns should be addressed in future studies. First, the heterogeneous reaction rates applied in this study were based on the available reports in the literature and the species evaluation was based on only one site in Beijing. Although the comparisons at one site are improved for the polluted days in Beijing, the sensitivity simulations on peak days indicated the current setting of the upper limit reaction rates might be still too low. Evaluations conducted using longer simulation periods of time and additional sites with observed speciated aerosol concentrations are needed to determine the appropriate heterogeneous reaction rates. Second, precursor emissions that are higher than available in the emission inventory due to special conditions might also be another factor contributing to the peak $PM_{2.5}$ events. Data assimilation techniques that use observed aerosol concentrations to constrain emission changes might also provide significant improvements in future studies.

**References**

Archer-Nicholls, S., Lowe, D., Utembe, S., Allan, J., Zaveri, R. A., Fast, J. D., Hodnebrog, O., van der Gon, H. D., and McFiggans, G.: Gaseous chemistry and aerosol mechanism developments for version 3.5.1 of the online regional model, WRF-Chem, Geosci. Model Dev., 7, 2557-2579, doi:10.5194/gmd-7-2557-2014, 2014.

Chen, H. S., Li, J., Ge, B. Z., Yang, W. Y., Wang, Z. F., Huang, S., Wang, Y. L., Yan, P. Z., Li, J. J., and Zhu, L. L.: Modeling study of source contributions and emergency control effects during a severe haze episode over the Beijing-Tianjin-Hebei area, Sci. China Chem., 58, 1403-1415, doi:10.1007/s11426-015-5458-y, 2015.

Chen, F., and Dudhia, J.: Coupling an advanced land surface-hydrology model with the Penn State-NCAR MM5 modeling system. Part I: Model implementation and sensitivity, Mon. Weather. Rev., 129, 569-585, doi:10.1175/1520-0493(2001)129<0569:Caalsh>2.0.Co;2, 2001.

Chou, M.-D., and M.J. Suarez.: An efficient thermal infrared radiation parameterization for use in general circulation models, NASA Tech. Memo., TM 104606, vol. 3, 25 pp., NASA Goddard Space Flight Cent., Greenbelt, Md. 1994

Cui, Y., Lin, J., Song, C., Liu, M., Yan, Y., Xu, Y., and Huang, B.: Rapid growth in nitrogen dioxide pollution over Western China, 2005–2013, Atmos. Chem. Phys., 16, 6207-6221, doi:10.5194/acp-16-6207-2016, 2016.

Dong, W., Xing, J., and Wang, S.: Temporal and spatial distribution of anthropogenic ammonia emissions in China:1994-200, Environ. Sci., 31, 1457-1463, 2010 (in Chinese)

Fast, J. D., Gustafson, W. I., Easter, R. C., Zaveri, R. A., Barnard, J. C., Chapman, E. G., Grell, G. A., and Peckham, S. E.: Evolution of ozone, particulates, and aerosol direct radiative forcing in the vicinity of Houston using a fully coupled meteorology-chemistry-aerosol model, J. Geophys. Res.-Atmos., 111, D21305, doi:10.1029/2005jd006721, 2006.

Grell, G. A., and Devenyi, D.: A generalized approach to parameterizing convection combining ensemble and data assimilation techniques, Geophys. Res. Lett., 29, Artn 1693. doi:10.1029/2002gl015311, 2002.

Grell, G. A., Peckham, S. E., Schmitz, R., McKeen, S. A., Frost, G., Skamarock, W. C., and Eder, B.: Fully coupled "online" chemistry within the WRF model, Atmos. Environ., 39, 6957-6975, doi:10.1016/j.atmosenv.2005.04.027, 2005.

Han, B., Zhang, R., Yang, W., Bai, Z., Ma, Z., and Zhang, W.: Heavy air pollution episodes in Beijing during January 2013: inorganic ion chemistry and source analysis using Highly Time-Resolved Measurements in an urban site, Atmos. Chem. Phys. Discuss., 15, 11111-11141, doi:10.5194/acpd-15-11111-2015, 2015.

He, K.B., Multi-resolution emission Inventory for China (MEIC): model framework and 1990-2010 anthropogenic emissions. In: Presented on the international Global Atmospheric Chemistry Conference, September 17-21, Beijing, China 2012

Hong, S. Y., Noh, Y., and Dudhia, J.: A new vertical diffusion package with an explicit treatment of entrainment processes, Mon. Weather. Rev., 134, 2318-2341, doi:10.1175/Mwr3199.1, 2006.

Huang, X., Song, Y., Li, M. M., Li, J. F., Huo, Q., Cai, X. H., Zhu, T., Hu, M., and Zhang, H. S.: A high-resolution ammonia emission inventory in China, Global Biogeochem. Cy., 26, Artn Gb1030. doi:10.1029/2011gb004161, 2012.

Jacob, D. J.: Heterogeneous chemistry and tropospheric ozone, Atmos. Environ., 34, 2131-2159, doi:10.1016/S1352-2310(99)00462-8, 2000.

Kim, J. Y., Song, C. H., Ghim, Y. S., Won, J. G., Yoon, S. C., Carmichael, G. R., and Woo, J. H.: An investigation on $NH_3$ emissions and particulate $NH_4+$-$NO_3$- formation in East Asia, Atmos. Environ., 40, 2139-2150, doi:10.1016/j.atmosenv.2005.11.048, 2006.

Krotkov, N. A., McLinden, C. A., Li, C., Lamsal, L. N., Celarier, E. A., Marchenko, S. V., Swartz, W. H., Bucsela, E. J., Joiner, J., Duncan, B. N., Boersma, K. F., Veefkind, J. P., Levelt, P. F., Fioletov, V. E., Dickerson, R. R., He, H., Lu, Z. F., and Streets, D. G.: Aura OMI observations of regional SO2 and NO2 pollution changes from 2005 to 2015, Atmos. Chem. Phys., 16, 4605-4629, doi:10.5194/acp-16-4605-2016, 2016.

Lamsal, L. N., Martin, R. V., Padmanabhan, A., van Donkelaar, A., Zhang, Q., Sioris, C. E., Chance, K., Kurosu, T. P., and Newchurch, M. J.: Application of satellite observations for timely updates to global anthropogenic $NO_x$ emission inventories, Geophys. Res. Lett., 38, Artn L05810. doi:10.1029/2010gl046476, 2011.

Lei, Y., Zhang, Q., He, K. B., and Streets, D. G.: Primary anthropogenic aerosol emission trends for China, 1990-2005, Atmos. Chem. Phys., 11, 931-954, doi:10.5194/acp-11-931-2011, 2011.

Li, W. J., and Shao, L. Y.: Transmission electron microscopy study of aerosol particles from the brown hazes in northern China, J. Geophys. Res.-Atmos., 114, Artn D09302. doi:10.1029/2008jd011285, 2009.

Li, W. J., and Shao, L. Y.: Characterization of mineral particles in winter fog of Beijing analyzed by TEM and SEM, Environ. Monit. Assess., 161, 565-573, doi:10.1007/s10661-009-0768-1, 2010.

Li, W. J., Zhou, S. Z., Wang, X. F., Xu, Z., Yuan, C., Yu, Y. C., Zhang, Q. Z., and Wang, W. X.: Integrated evaluation of aerosols from regional brown hazes over northern China in winter: Concentrations, sources, transformation, and mixing states, J. Geophys. Res.-Atmos., 116, Artn D09301. doi:10.1029/2010jd015099, 2011.

Li, M., Zhang, Q., Streets, D. G., He, K. B., Cheng, Y. F., Emmons, L. K., Huo, H., Kang, S. C., Lu, Z., Shao, M., Su, H., Yu, X., and Zhang, Y.: Mapping Asian anthropogenic emissions of non-methane volatile organic compounds to multiple chemical mechanisms, Atmos. Chem. Phys., 14, 5617-5638, doi:10.5194/acp-14-5617-2014, 2014.

Liu, X. G., Li, J., Qu, Y., Han, T., Hou, L., Gu, J., Chen, C., Yang, Y., Liu, X., Yang, T., Zhang, Y., Tian, H., and Hu, M.: Formation and evolution mechanism of regional haze: a case study in the megacity Beijing, China, Atmos. Chem. Phys., 13, 4501-4514, doi:10.5194/acp-13-4501-2013, 2013.

Lu, Z., Zhang, Q., and Streets, D. G.: Sulfur dioxide and primary carbonaceous aerosol emissions in China and India, 1996-2010, Atmos. Chem. Phys., 11, 9839-9864, doi:10.5194/acp-11-9839-2011, 2011.

Lupascu, A., Easter, R., Zaveri, R., Shrivastava, M., Pekour, M., Tomlinson, J., Yang, Q., Matsui, H., Hodzic, A., Zhang, Q., and Fast, J. D.: Modeling particle nucleation and growth over northern California during the 2010 CARES campaign, Atmos. Chem. Phys., 15, 12283-12313, doi:10.5194/acp-15-12283-2015, 2015.

McKeen, S. A., Wotawa, G., Parrish, D. D., Holloway, J. S., Buhr, M. P., Hubler, G., Fehsenfeld, F. C., and Meagher, J. F.: Ozone production from Canadian wildfires during June and July of 1995, J. Geophys. Res.-Atmos., 107, 4192, doi:10.1029/2001jd000697, 2002.

Mlawer, E. J., Taubman, S. J., Brown, P. D., Iacono, M. J., and Clough, S. A.: Radiative transfer for inhomogeneous atmospheres: RRTM, a validated correlated-k model for the longwave, J Geophys Res-Atmos, 102, 16663-16682, doi:10.1029/97jd00237, 1997.

Richter, A., Burrows, J. P., Nuss, H., Granier, C., and Niemeier, U.: Increase in tropospheric nitrogen dioxide over China observed from space, Nature, 437, 129-132, doi:10.1038/nature04092, 2005.

Shi, Y., Xia, Y. F., Lu, B. H., Liu, N., Zhang, L., Li, S. J., and Li, W.: Emission inventory and trends of NO (x) for China, 2000-2020, J. Zhejiang Univ-Sc. A, 15, 454-464, doi:10.1631/jzus.A1300379, 2014.

Streets, D. G., Bond, T. C., Carmichael, G. R., Fernandes, S. D., Fu, Q., He, D., Klimont, Z., Nelson, S. M., Tsai, N. Y., Wang, M. Q., Woo, J. H., and Yarber, K. F.: An inventory of gaseous and primary aerosol emissions in Asia in the year 2000, J. Geophys. Res.-Atmos., 108, Artn 8809. doi:10.1029/2002jd003093, 2003.

Sun, Y. L., Zhuang, G. S., Tang, A. H., Wang, Y., and An, Z. S.: Chemical characteristics of $PM_{2.5}$ and $PM_{1}0$ in haze-fog episodes in Beijing, Environ. Sci. Technol., 40, 3148-3155, doi:10.1021/es051533g, 2006.

Sun, Y. L., Wang, Z. F., Fu, P. Q., Yang, T., Jiang, Q., Dong, H. B., Li, J., and Jia, J. J.: Aerosol composition, sources and processes during wintertime in Beijing, China, Atmos. Chem. Phys., 13, 4577-4592, doi:10.5194/acp-13-4577-2013, 2013.

Sun, Y. L., Wang, Z. F., Du, W., Zhang, Q., Wang, Q. Q., Fu, P. Q., Pan, X. L., Li, J., Jayne, J., and Worsnop, D. R.: Long-term real-time measurements of aerosol particle composition in Beijing, China: seasonal variations, meteorological effects, and source analysis, Atmos. Chem. Phys., 15, 10149-10165, doi:10.5194/acp-15-10149-2015, 2015.

Wang, K., Zhang, Y., Nenes, A., and Fountoukis, C.: Implementation of dust emission and chemistry into the Community Multiscale Air Quality modeling system and initial application to an Asian dust storm episode, Atmos. Chem. Phys., 12, 10209-10237, doi:10.5194/acp-12-10209-2012, 2012a.

Wang, X. F., Wang, W. X., Yang, L. X., Gao, X. M., Nie, W., Yu, Y. C., Xu, P., Zhou, Y., and Wang, Z.: The secondary formation of inorganic aerosols in the droplet mode through heterogeneous aqueous reactions under haze conditions, Atmos. Environ., 63, 68-76, doi:10.1016/j.atmosenv.2012.09.029, 2012b.

Wang, Y., Zhang, Q. Q., He, K., Zhang, Q., and Chai, L.: Sulfate-nitrate-ammonium aerosols over China: response to 2000-2015 emission changes of sulfur dioxide, nitrogen oxides, and ammonia, Atmos. Chem. Phys., 13, 2635-2652, doi:10.5194/acp-13-2635-2013, 2013.

Wang, L. T., Wei, Z., Yang, J., Zhang, Y., Zhang, F. F., Su, J., Meng, C. C., and Zhang, Q.: The 2013 severe haze over southern Hebei, China: model evaluation, source apportionment, and policy implications, Atmos. Chem. Phys., 14, 3151-3173, doi:10.5194/acp-14-3151-2014, 2014a.

Wang, L. T., Zhang, Y., Wang, K., Zheng, B., Zhang, Q., and Wei, W.: Application of Weather Research and Forecasting Model with Chemistry (WRF/Chem) over northern China: Sensitivity study, comparative evaluation, and policy implications, Atmos. Environ., 124, 337-350, doi:10.1016/j.atmosenv.2014.12.052, 2016.

Wang, W., Maenhaut, W., Yang, W., Liu, X. D., Bai, Z. P., Zhang, T., Claeys, M., Cachier, H., Dong, S. P., and Wang, Y. L.: One-year aerosol characterization study for $PM_{2.5}$ and $PM_10$ in Beijing, Atmos. Pollut. Res., 5, 554-562, doi:10.5094/Apr.2014.064, 2014b.

Wang, Y. S., Yao, L., Wang, L. L., Liu, Z. R., Ji, D. S., Tang, G. Q., Zhang, J. K., Sun, Y., Hu, B., and Xin, J. Y.: Mechanism for the formation of the January 2013 heavy haze pollution episode over central and eastern China, Sci. China Earth Sci., 57, 14-25, doi:10.1007/s11430-013-4773-4, 2014c.

Wang, Y. X., Zhang, Q. Q., Jiang, J. K., Zhou, W., Wang, B. Y., He, K. B., Duan, F. K., Zhang, Q., Philip, S., and Xie, Y. Y.: Enhanced sulfate formation during China's severe winter haze episode in January 2013 missing from current models, J. Geophys. Res.-Atmos., 119, doi:10.1002/2013JD021426, 2014d.

Wang, S. W., Zhang, Q., Martin, R. V., Philip, S., Liu, F., Li, M., Jiang, X. J., and He, K. B.: Satellite measurements oversee China's sulfur dioxide emission reductions from coal-fired power plants, Environ. Res. Lett., 10, Artn 114015. doi:10.1088/1748-9326/10/11/114015, 2015.

Wen, L. A., Chen, J. M., Yang, L. X., Wang, X. F., Xu, C. H., Sui, X. A., Yao, L., Zhu, Y. H., Zhang, J. M., Zhu, T., and Wang, W. X.: Enhanced formation of fine particulate nitrate at a rural site on the North China Plain in summer: The important roles of ammonia and ozone, Atmos. Environ., 101, 294-302, doi:10.1016/j.atmosenv.2014.11.037, 2015.

Wild, O., Zhu, X., and Prather, M. J.: Fast-j: Accurate simulation of in- and below-cloud photolysis in tropospheric chemical models, J Atmos Chem, 37, 245-282, doi:10.1023/A:1006415919030, 2000.

Xia, Y. M., Zhao, Y., and Nielsen, C. P.: Benefits of of China's efforts in gaseous pollutant control indicated by the bottom-up emissions and satellite observations 2000-2014, Atmos. Environ., 136, 43-53, doi:10.1016/j.atmosenv.2016.04.013, 2016.

Xu, P., Zhang, Y. S., Gong, W. W., Hou, X. K., Kroeze, C., Gao, W., and Luan, S. J.: An inventory of the emission of ammonia from agricultural fertilizer application in China for 2010 and its high-resolution spatial distribution, Atmos. Environ., 115, 141-148, doi:10.1016/j.atmosenv.2015.05.020, 2015.

Yang, Y. R., Liu, X. G., Qu, Y., An, J. L., Jiang, R., Zhang, Y. H., Sun, Y. L., Wu, Z. J., Zhang, F., Xu, W. Q., and Ma, Q. X.: Characteristics and formation mechanism of continuous hazes in China: a case study during the autumn of 2014 in the North China Plain, Atmos. Chem. Phys., 15, 8165-8178, doi:10.5194/acp-15-8165-2015, 2015.

Zaveri, R. A., and Peters, L. K.: A new lumped structure photochemical mechanism for large-scale applications, J Geophys Res-Atmos, 104, 30387-30415, doi:10.1029/1999jd900876, 1999.

Zaveri, R. A., Easter, R. C., Fast, J. D., and Peters, L. K.: Model for Simulating Aerosol Interactions and Chemistry (MOSAIC), J. Geophys. Res.-Atmos., 113, D13204, doi:10.1029/2007jd008782, 2008.

Zhang, Y., Dore, A. J., Ma, L., Liu, X. J., Ma, W. Q., Cape, J. N., and Zhang, F. S.: Agricultural ammonia emissions inventory and spatial distribution in the North China Plain, Environ. Pollut., 158, 490-501, doi:10.1016/j.envpol.2009.08.033, 2010.

Zhang, Q., Streets, D. G., Carmichael, G. R., He, K. B., Huo, H., Kannari, A., Klimont, Z., Park, I. S., Reddy, S., Fu, J. S., Chen, D., Duan, L., Lei, Y., Wang, L. T., and Yao, Z. L.: Asian emissions in 2006 for the NASA INTEX-B mission, Atmos. Chem. Phys., 9, 5131-5153, doi:10.5194/acp-9-5131-2009, 2009.

Zhang, Q., Geng, G. N., Wang, S. W., Richter, A., and He, K. B.: Satellite remote sensing of changes in NO (x) emissions over China during 1996-2010, Chinese Sci. Bull., 57, 2857-2864, doi:10.1007/s11434-012-5015-4, 2012.

Zhang, L., Wang, T., Lv, M. Y., and Zhang, Q.: On the severe haze in Beijing during January 2013: Unraveling the effects of meteorological anomalies with WRF-Chem, Atmos. Environ., 104, 11-21, doi:10.1016/j.atmosenv.2015.01.001, 2015a.

Zhang, L., Liu, L. C., Zhao, Y. H., Gong, S. L., Zhang, X. Y., Henze, D. K., Capps, S. L., Fu, T. M., Zhang, Q., and Wang, Y. X.: Source attribution of particulate matter pollution over North China with the adjoint method, Environ. Res. Lett., 10, Artn 084011. doi:10.1088/1748-9326/10/8/084011, 2015b.

Zhang, Y., and Carmichael, G. R.: The role of mineral aerosol in tropospheric chemistry in East Asia - A model study, J. Appl. Meteorol., 38, 353-366, doi:10.1175/1520-0450(1999)038<0353:Tromai>2.0.Co;2, 1999.

Zhao, X. J., Zhao, P. S., Xu, J., Meng, W., Pu, W. W., Dong, F., He, D., and Shi, Q. F.: Analysis of a winter regional haze event and its formation mechanism in the North China Plain, Atmos. Chem. Phys., 13, 5685-5696, doi:10.5194/acp-13-5685-2013, 2013.

Zheng, B., Zhang, Q., Zhang, Y., He, K. B., Wang, K., Zheng, G. J., Duan, F. K., Ma, Y. L., and Kimoto, T.: Heterogeneous chemistry: a mechanism missing in current models to explain secondary inorganic aerosol formation during the January 2013 haze episode in North China, Atmos. Chem. Phys., 15, 2031-2049, doi:10.5194/acp-15-2031-2015, 2015.
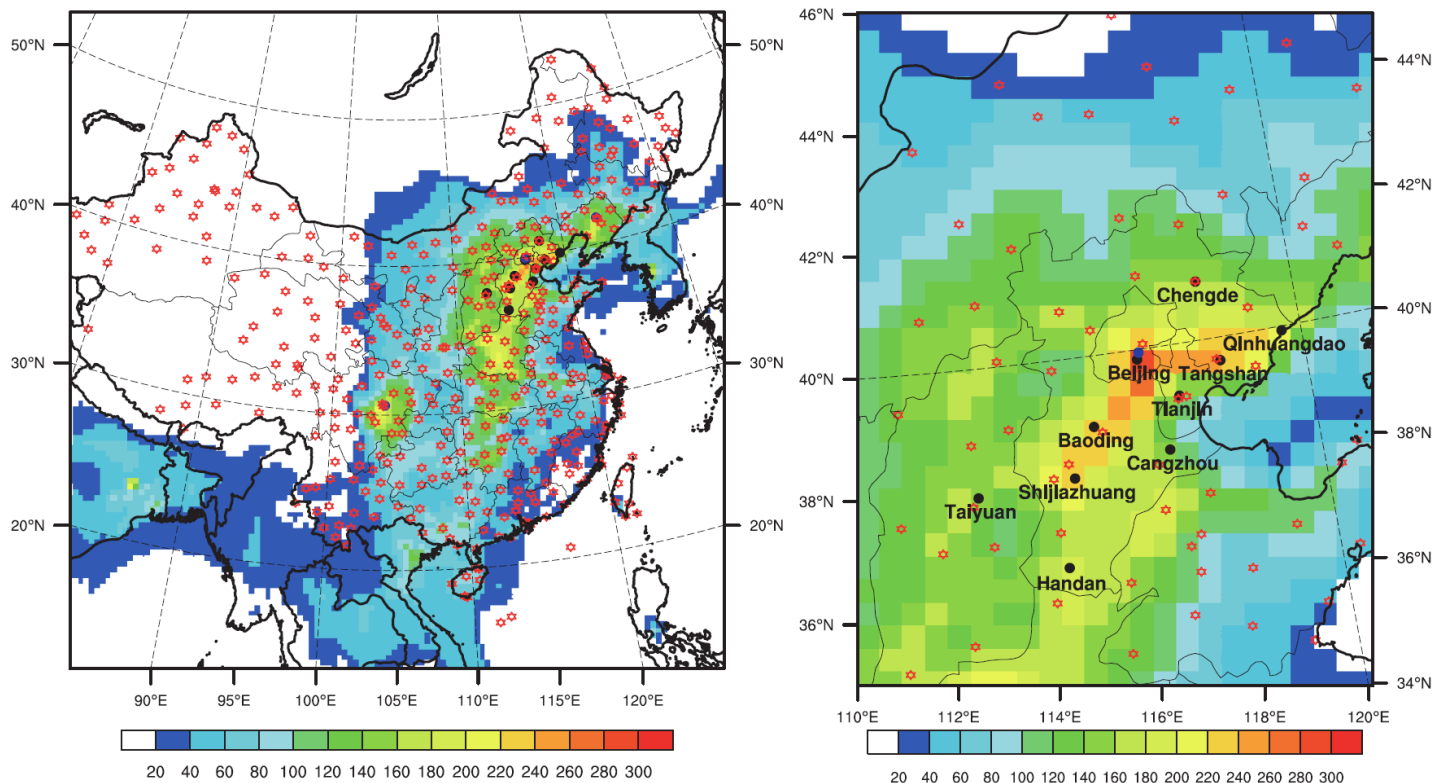
**Figure 1.** The model domain and (left panel) and the Northern China Plain (NCP, right panel). Dots are the observational sites, where red denotes NCDC meteorological sites, blue denotes the Beijing Normal University (BNU) site, black denotes AQI national monitoring sites. Shaded backgrounds are model-simulated $PM_{2.5}$ concentrations ($\mu g\ m^{-3}$) that illustrate the regional pollution on October 10.
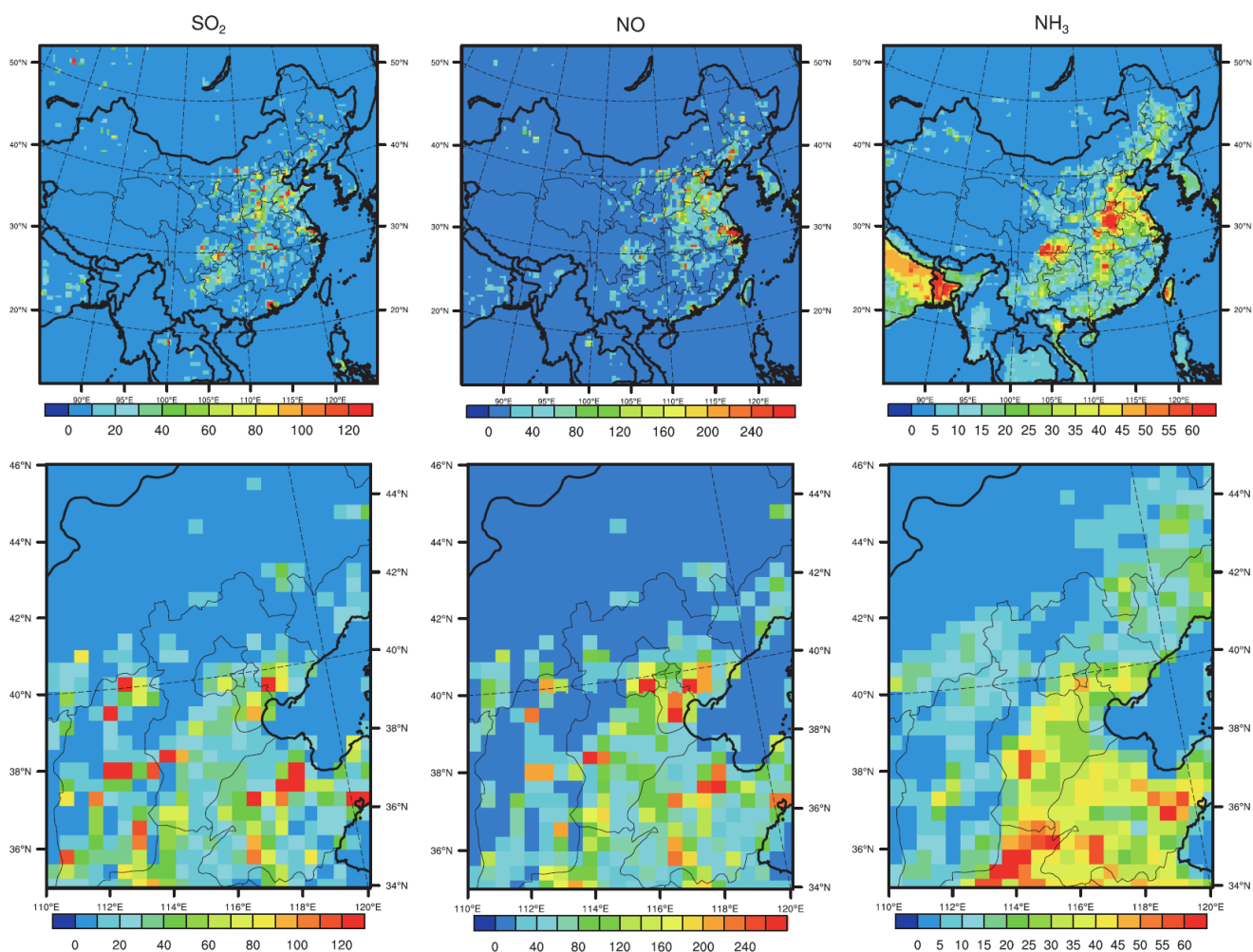
**Figure 2.** Spatial distribution of SO$_2$ (left), NO (middle) and NH$_3$ (right) emissions over the model domain (top panels) and in NCP (bottom panels). Units are in mol km$^{-2}$ hr$^{-1}$.
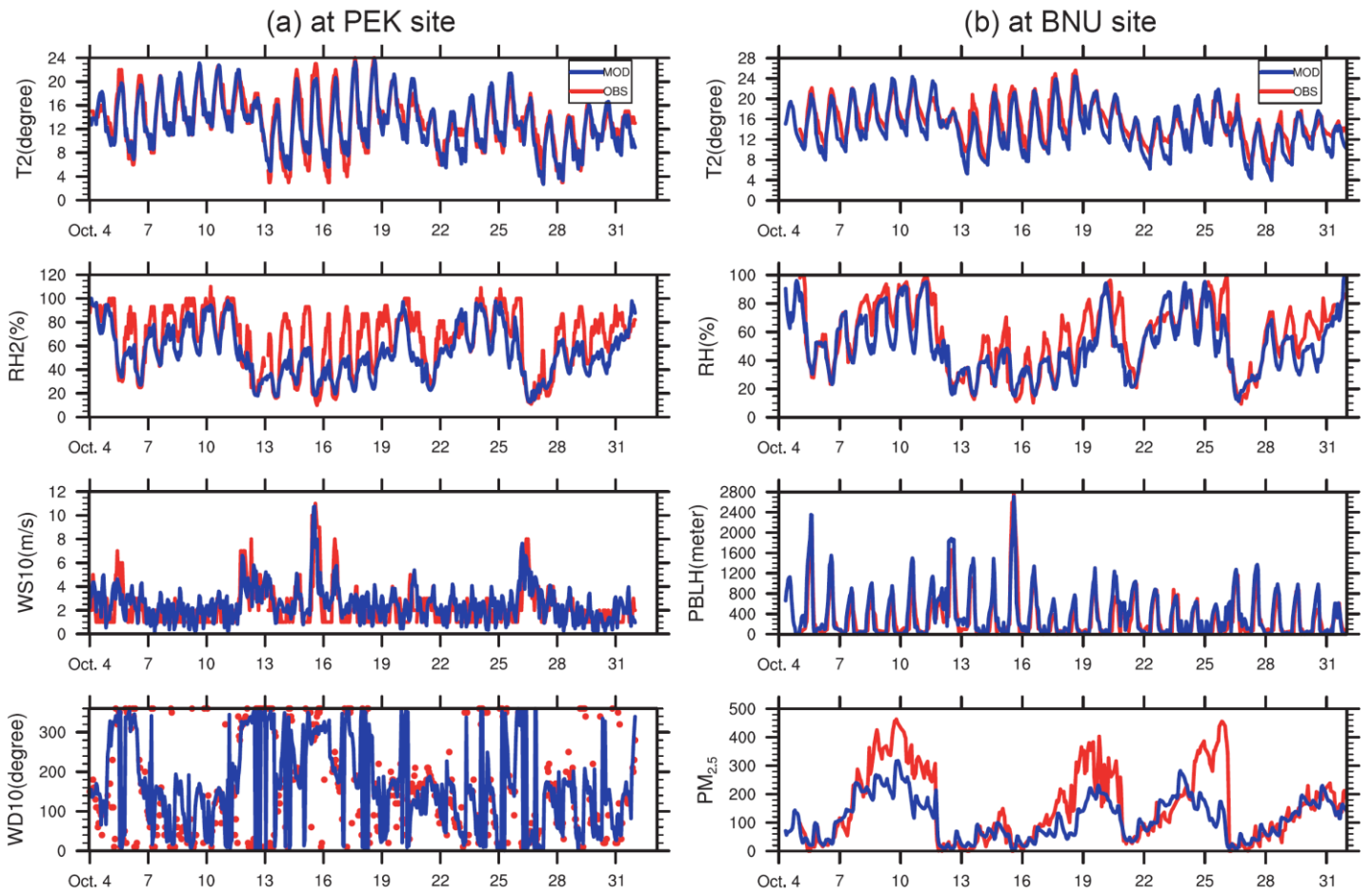
**Figure 3.** Time series of observed and simulated meteorological parameters and PM$_{2.5}$ at the (a) PEK and (b) the BNU sites (in local time). Time starts at 00:00 local time. Parameters: T2- temperature at 2 meter (degree), RH2- relative humidity at 2 meter (%), WS10- wind speed at 10 meter (m/s), WD10- wind direction at 10 meter (degree) and PBLH- planetary boundary layer height (meter).
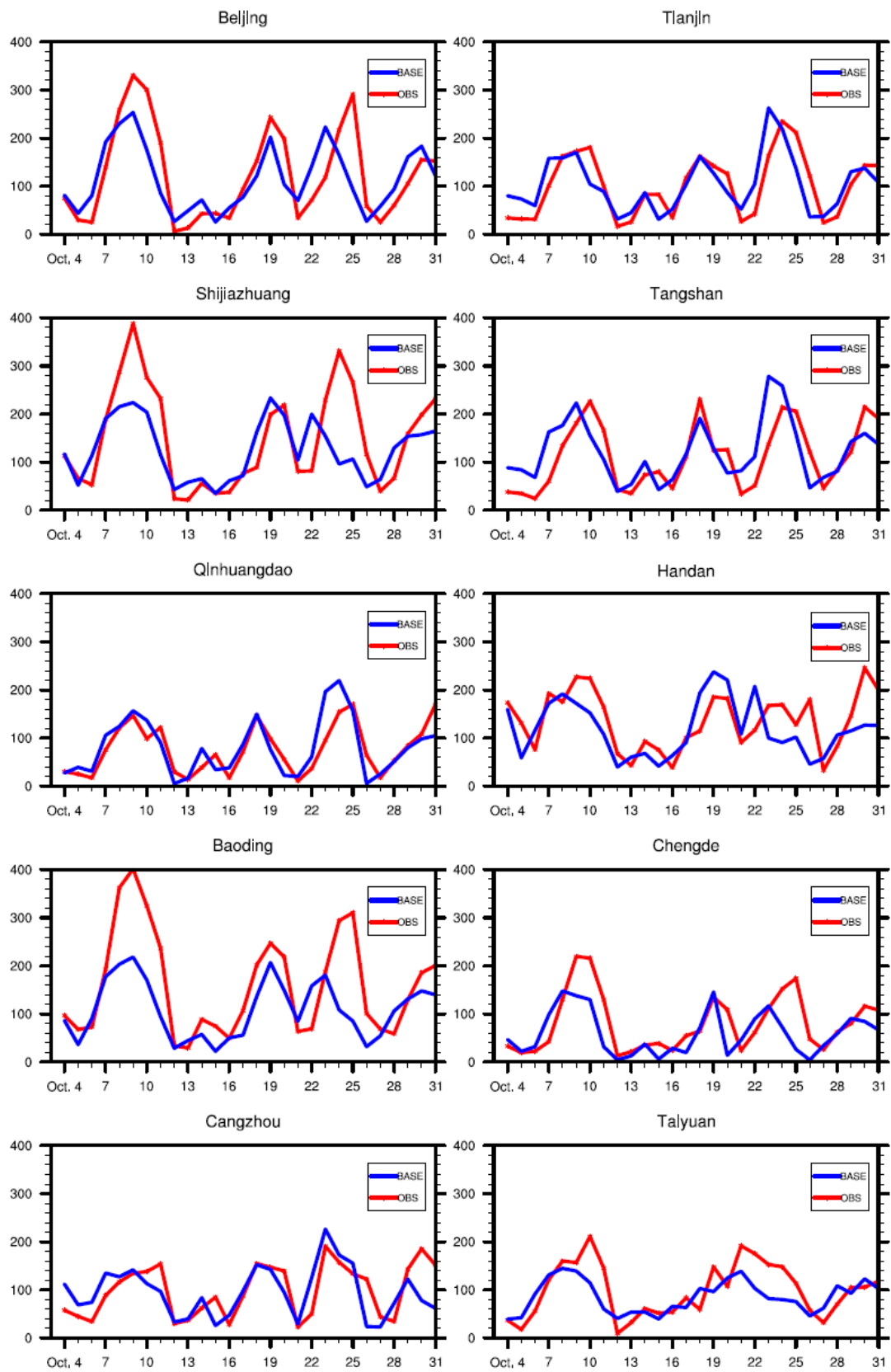
**Figure 4.** Time series of observed 24-hour averaged PM$_{2.5}$ concentrations (μg m$^{-3}$) at 10 national monitoring system sites in the NCP (locations as black dots in Fig. 1), along with the results from the BASE simulation.
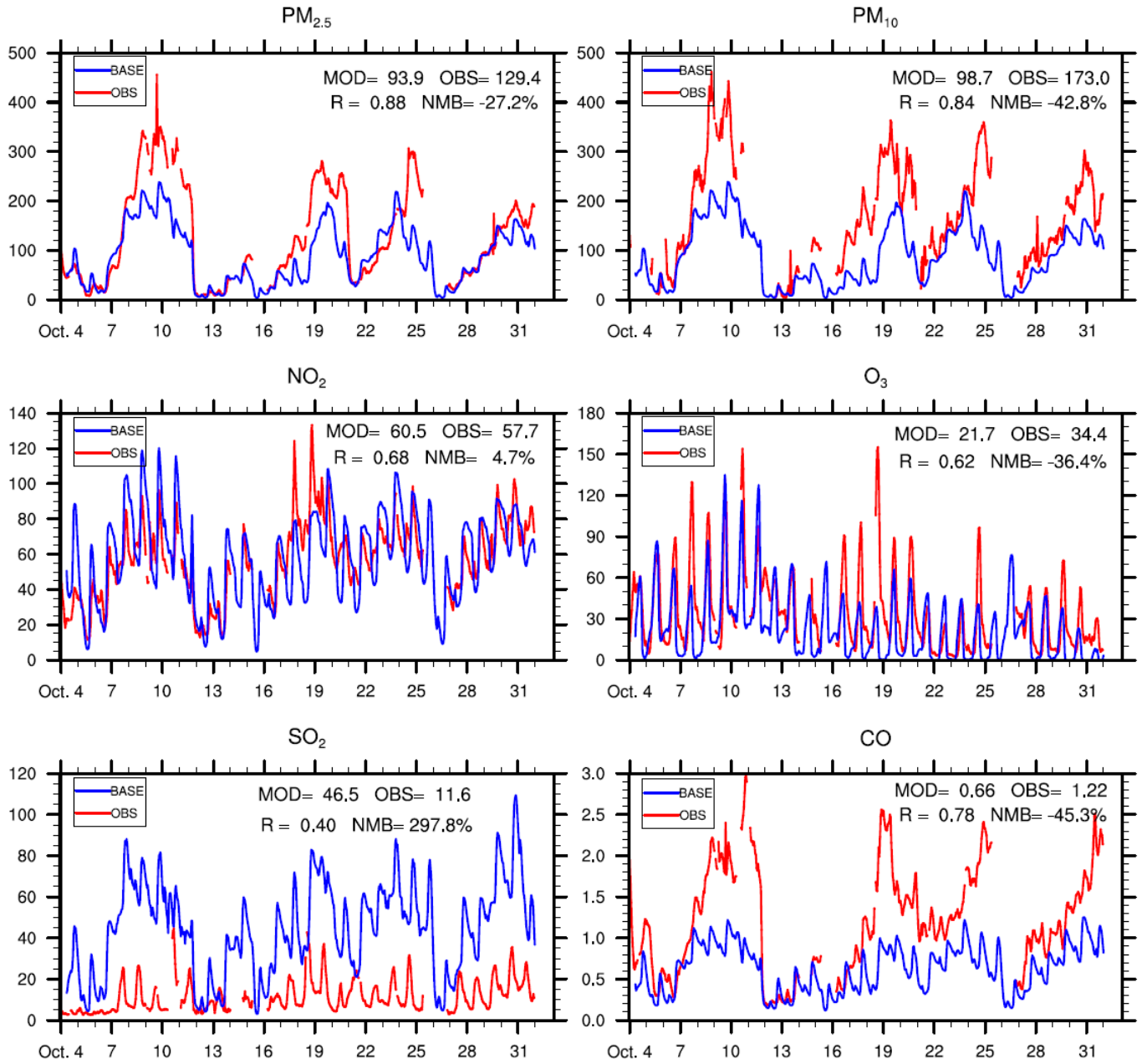
**Figure 5.** Time series of observed averaged pollutants concentrations at 34 sites in Beijing (from local monitoring system) along with the results from the BASE simulation. Units are mg m$^{-3}$ for CO and μg m$^{-3}$ for the other panels.
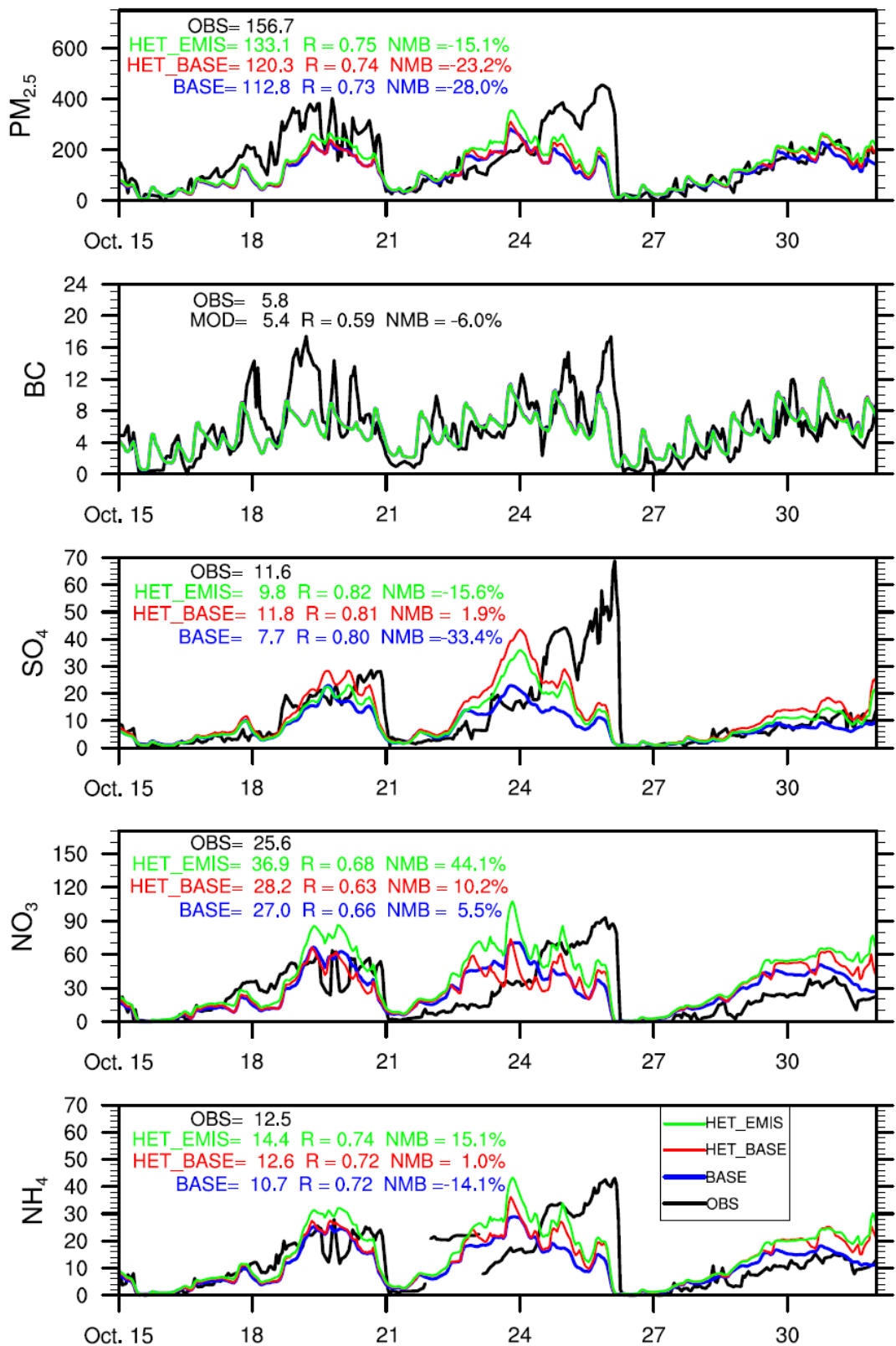
**Figure 6.** Time series of observed (OBS) and simulated (BASE, HET_BASE, HET_EMIS) hourly PM$_{2.5}$ and PM$_1$ species ($\mu$g m$^{-3}$) including black carbon (BC), sulfate (SO$_4$), nitrate (NO$_3$) and ammonium (NH$_4$). Descriptions of model scenarios are given in Table 3.
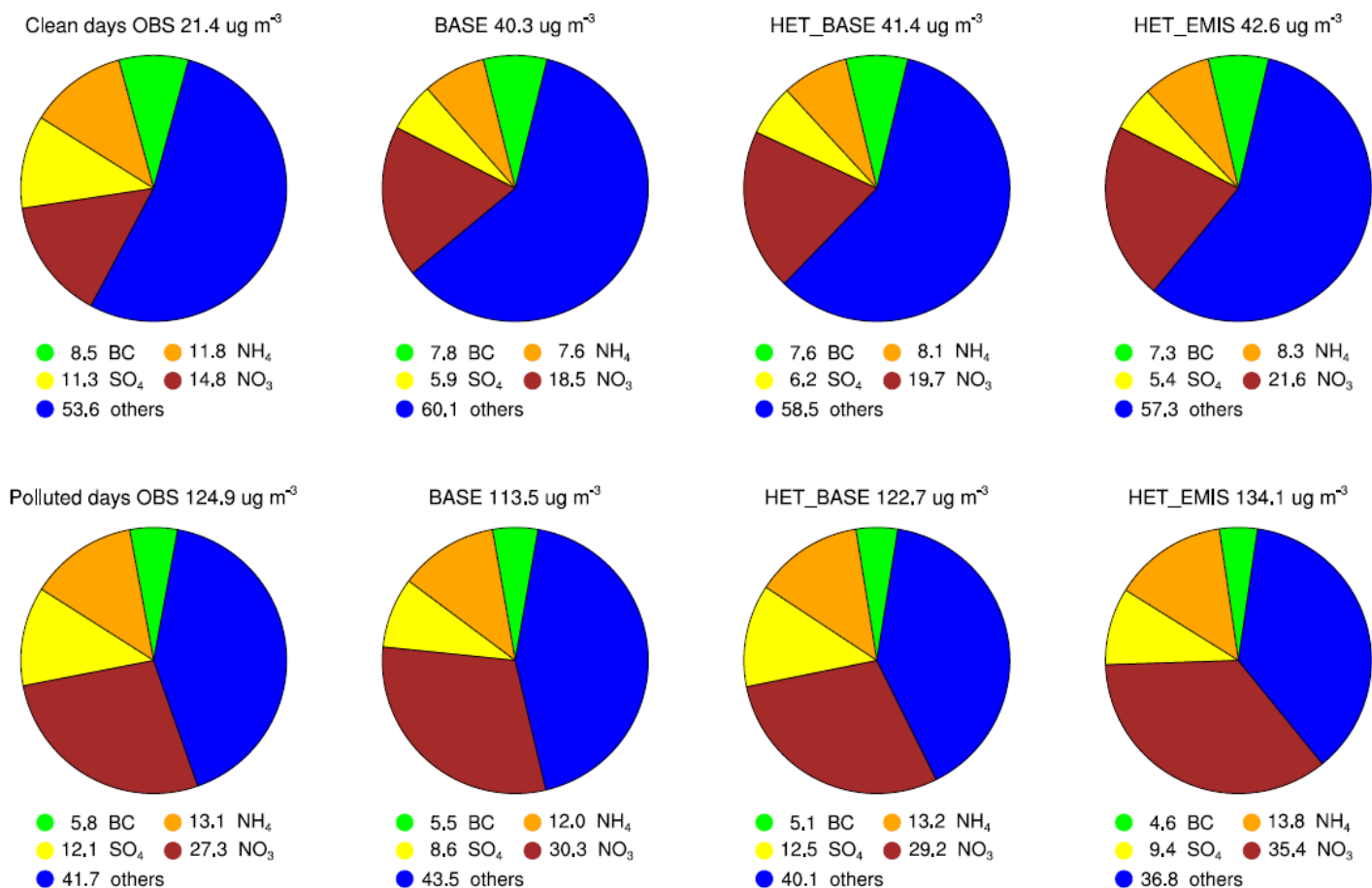
**Figure 7.** Pie charts of observed and simulated mass fractions of $PM_1$ species on relatively clean days (observed $PM_{2.5} < 75$ μg m$^{-3}$) and polluted days (observed $PM_{2.5} >= 75$ μg m$^{-3}$) between the October 15-31. The units of total $PM_1$ concentrations (listed in panel titles) are μg m$^{-3}$. The species fractions (listed in panel labels) are in percentage (%).
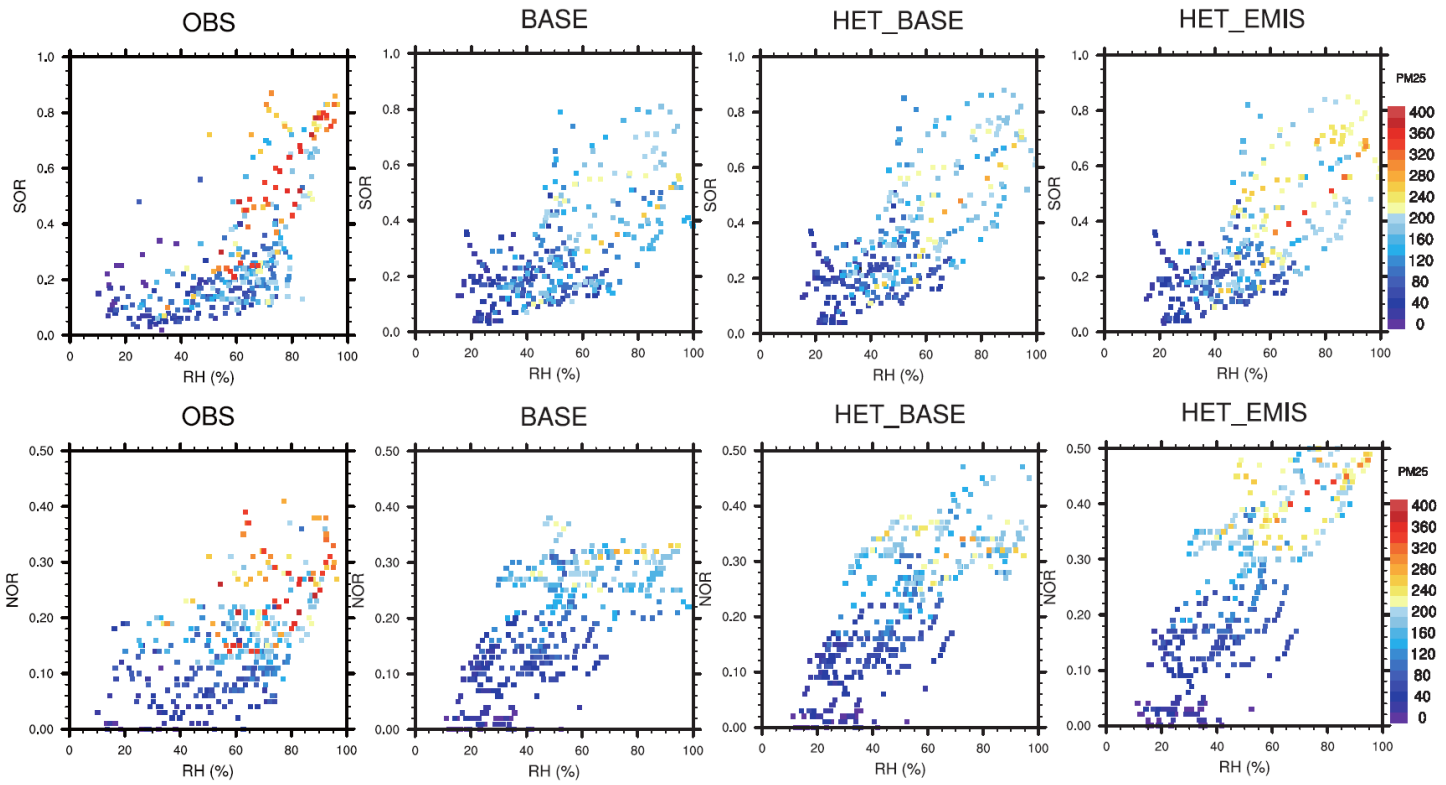
**Figure 8.** Observed (OBS) and simulated (BASE, HET_BASE, HET_EMIS) sulfur (SOR) and nitric (NOR) oxidation rates in $PM_1$ between October 15-31. The x-axis is the observed for left panels and simulated relative humidity for the other panels. Colors denote different $PM_{2.5}$ concentrations ($\mu g\ m^{-3}$).
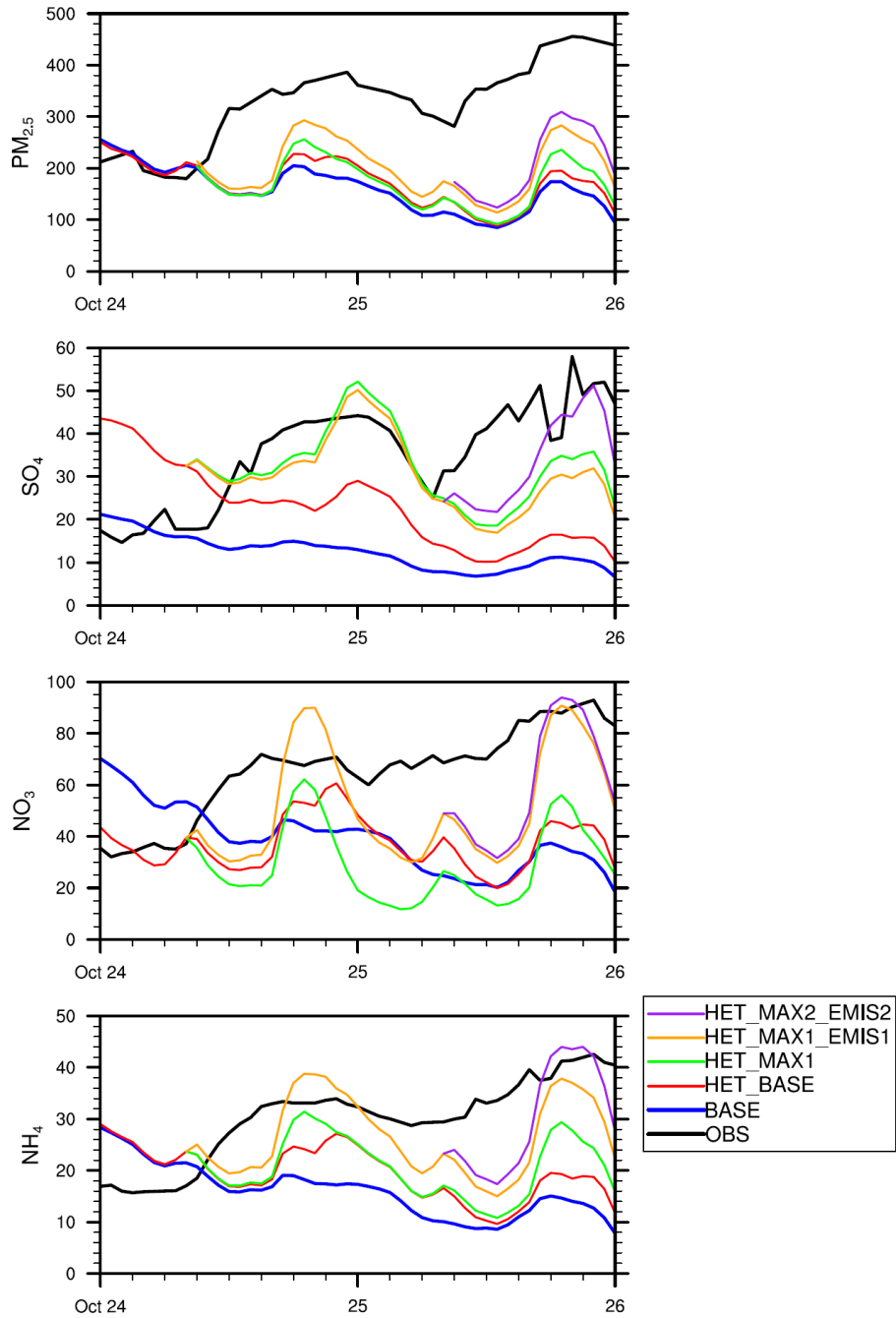
**Figure 9.** The sensitivity simulations of PM$_{2.5}$ and SNA species ( µg m$^{-3}$) for the October 24-25 pollution period.
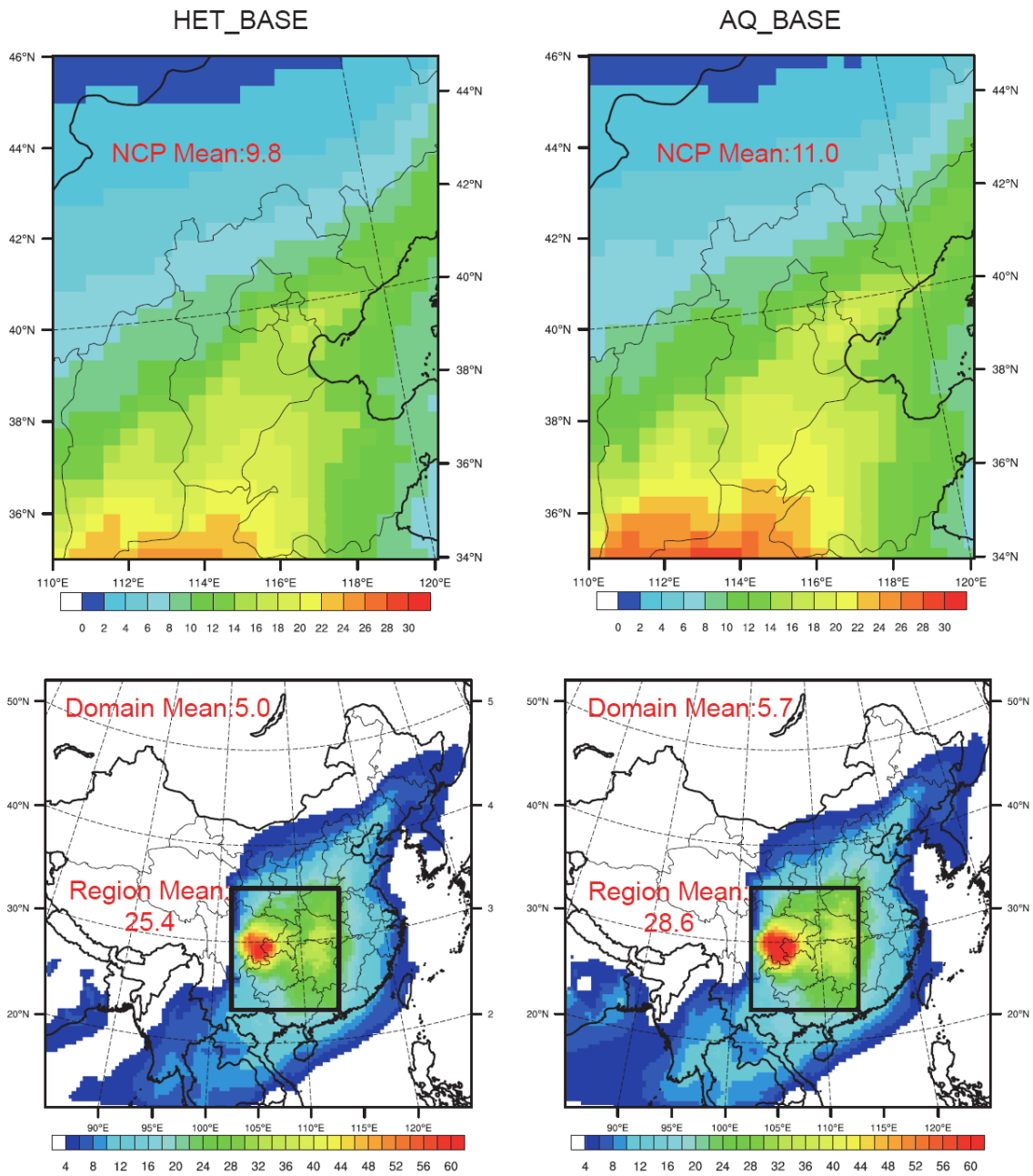
Figure 10. Spatial distribution of mean sulfate (in PM$_{2.5}$) from HET_BASE and AQ_BASE (units: μg m$^{-3}$) for the period of Oct. 15-31, 2014.
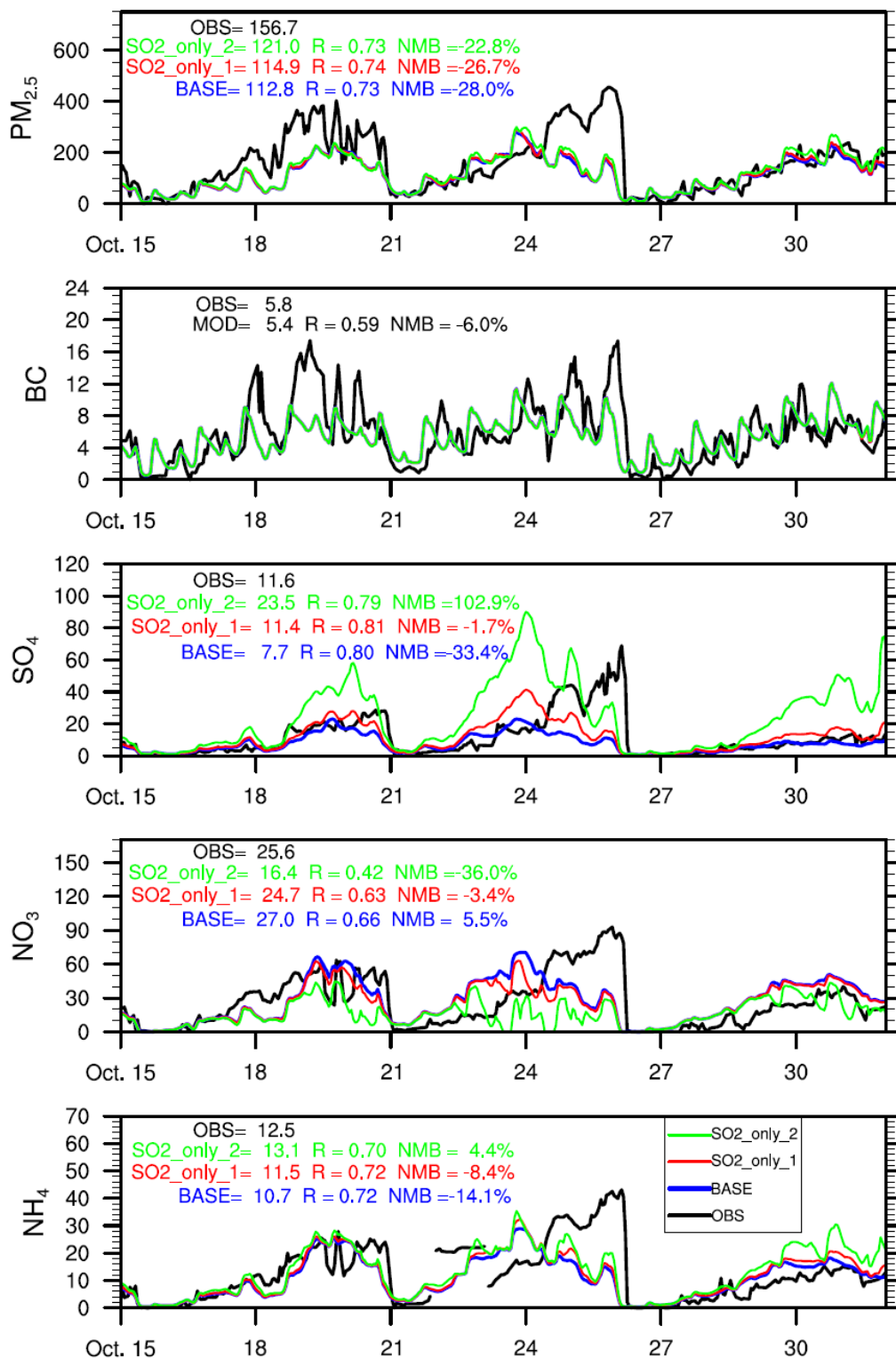
Figure S1. Same as Figure 6 but for the BASE, SO2_only_1, and SO2_only_2 simulations (units: µg m$^{-3}$). SO2_only_1 with lower/upper limits $2 \times 10^{-5}/5 \times 10^{-5}$; SO2_only_2 with lower/upper limits $1.0 \times 10^{-4}/2.6 \times 10^{-4}$.